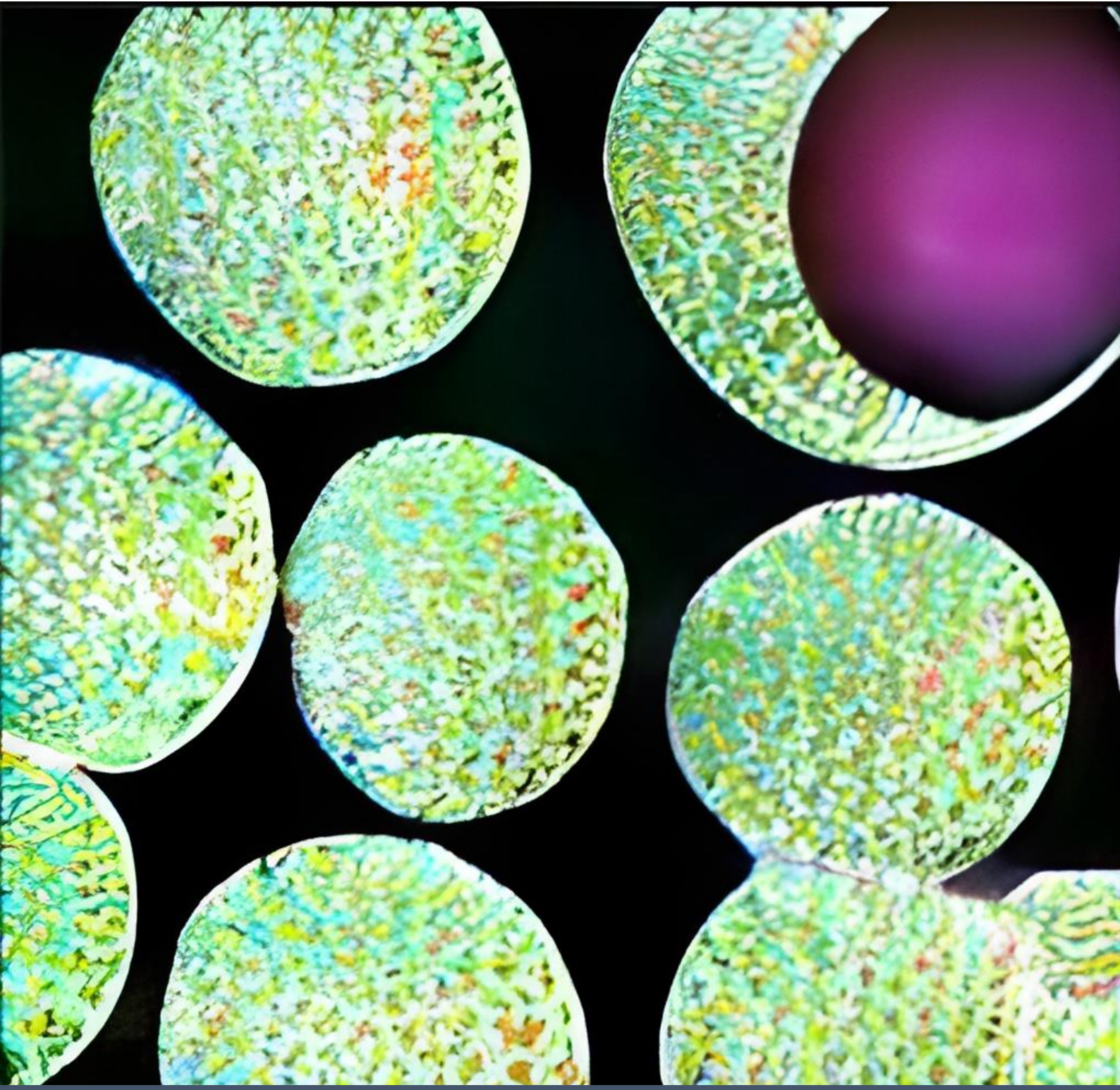

Polymeric micelles as carriers for a ^{166}Dy/^{166}Ho *in vivo* generator

Catalina Villarreal Gómez

TU Delft

Polymeric micelles as carriers for a ^{166}Dy/^{166}Ho *in vivo* generator

By

Catalina Villarreal Gómez

in partial fulfilment of the requirements for the degree of

Master of Science
in Chemical Engineering

at the Delft University of Technology,
to be defended publicly on **6th July 2022** at **09h30**.

Supervisor:	Dr. A.G. Denkova	TU Delft
Thesis committee:	Dr. K Djanashvili,	TU Delft
	Dr. R Eelkema,	TU Delft

TU Delft

Abstract

Cancer is one of the leading causes of death in the world. Because of this, there are many novel methods to treat it being currently researched. One of the answers from the nuclear medicine perspective is Radionuclide Therapy, where alpha or beta emitters are applied, with the goal to selectively irradiate tumours in the body. A promising radionuclide researched for Radionuclide Therapy is Holmium-166, which is a beta emitter with a short half-life of 26.8 hours, which is useful for the treatment of large metastases. A method to ensure an effective treatment with Holmium-166 is the use of a Dysprosium-166/Holmium-166 *in vivo* generator, as the dose delivered to patients per administered dose is two times higher with the *in vivo* generator rather than the direct use of Holmium-166. However, carriers used in Radionuclide Therapy, which usually involve the formation of a chelator-metal complex are not effective for the *in vivo* generator due to the release of auger electrons during the decay process leading to the destruction of the chelator-metal complex. A promising non-chelator method designed by Liu et al. at the Applied Radiation and Isotopes research team at TU Delft involves the radiolabelling of micelles. This thesis sought to evaluate the use of micelles, radiolabelled with this mechanism as an effective carrier for the Dysprosium-166/Holmium-166 *in vivo* generator. For this, micelles made of Polycaprolactone-block-Polyethylene Oxide and Polylactic Acid-block-Polyethylene oxide were evaluated based on the obtained radiolabelling efficiency and their stability when challenged with diethylenetriaminepentaacetic acid (DTPA). The results in this study show that the radiolabelling method used to encapsulate Dysprosium relies on the diffusion of Dysprosium hydroxides into the micelle core, followed by precipitation as the right concentration is reached inside the micelles. The best results obtained by this study occur when radiolabelling Polylactic Acid-block-Polyethylene Oxide (PLA-PEO) micelles, and then adding phosphate ions at a concentration of $3 \times 10^{-8} M$, 30 minutes after the addition of the active Dysprosium. Although more tuning is required on the radiolabelling mechanism to make micelles the most effective carriers of the ^{166}Dy/^{166}Ho *in vivo* generator, promising first steps were made to begin this process.

Acknowledgements

I cannot believe that I am at a point where I am writing the acknowledgements to my Master thesis. It has been a very interesting 9 months, and I have learned a lot about myself and everything I work for. I am very happy to be able to present this to whoever you are as a show that satisfaction comes out of hard work.

There are a lot of people who were absolutely vital to the completion of my thesis, and I would not be here, on the other side, if it weren't for them.

First and foremost, I would like to thank Dr. Ir Antonia Denkova for everything. It was an honour to work under your supervision and to always have discussions where I always felt free to say anything, and that we were talking as equals, both in interest and willingness to come up with ideas and solutions. Thank you for your patience and for your attention, even at times when I did not expect them. Finally, thank you for making sure the end was not too overwhelming for me and for always being on top of all our conversations.

To Runze Wang and Dr. Huanhuan Liu, I am eternally grateful for all your help. Your readiness to answer any question I had and help me with anything I needed, as well as your ability to calm me down when I was slightly overwhelmed was invaluable for me to get as far as I did in my project. You taught me a lot and you trained me well to make my research great.

To my committee, Dr Kristina Djanashvili and Dr. Rienk Eelkema, I appreciate your readiness to move my defence date, and I am honoured to be evaluated by you both. I hope this work will be as interesting to you as it was for me to finish!

To Baukje and Astrid, thank you for making sure I was ready and able to work independently in the lab, and for all your help training me to use the equipment I needed, and to always get my activity on time.

To Eline, thank you for all the chats and nice times in and out of the lab, and for giving me small extra adventures along the way.

To the rest of our research team at ARI (both people who are currently still here and people who already finished), thank you for all the nice times, for sometimes forcing me to take breaks and make sure to hydrate, and for making Fridays a great event always! I think you all helped in making my Dutch a bit better (even if you never heard me speak it) and you always made me smile when I joined team activities, be it just having coffee, or going bowling.

To all of my family, but especially my parents, Mosi and my uncle Francisco and aunt Emanuela, your unconditional support (even though it is from afar) is the reason why I am here and thriving and I love you all so much! Despite the long distance, talking to you always brings a smile to my face and I appreciate every single call and every single laugh we get together.

To Ferran, thank you for always being there for me, with all the patience of a saint, and for always giving me the comfort I needed to continue.

Finally, to the family I found along the way, Silvi, Pabs, Sap, and everyone at Breestraat 9 (current and former), I would not be sane all the way across the pond without you guys. Every single outing, dinner, party and fun time made me feel like I could have it all.

I am extremely grateful for every moment, and every memory that led us here, to this accomplishment, that shows that with a bit of patience and a lot of work, you can achieve greatness.

Catalina Villarreal Gómez, 2022

Table of Contents

List of Figures

List of Tables

List of Abbreviations and Symbols

Dysprosium species

Dy	Dysprosium
Dy(III)	Dysprosium
^{164}Dy	Dysprosium-164
^{166}Dy	Dysprosium-166
$^{166}Dy/^{166}Ho$	Dysprosium-166/Holmium-166
Dy^{3+}	Dysprosium 3+ ion
$DyCl^{2+}$	Dysprosium chloride 2+ ion
$DyCl_2^{+}$	Dysprosium chloride + ion
$DyCl_3.6H_2O$	Dysprosium chloride hexahydrate
$Dy(OH)_{3\ (aq)}$	Aqueous Dysprosium hydroxide
$Dy(OH)^{2+}$	Dysprosium hydroxide 2+ ion
$Dy(OH)_2^{+}$	Dysprosium hydroxide + ion
$Dy(OH)_4^{-}$	Dysprosium hydroxide - ion
$Dy(OH)_{3\ (s)}$	Solid Dysprosium hydroxide
$Dy(NO_3)^{2+}$	Dysprosium nitrate 2+ ion
$Dy(NO_3)_3.5H_2O$	Dysprosium nitrate pentahydrate
Dy_2O_3	Dysprosium oxide
$Dy(PO_4)_{(s)}$	Solid Dysprosium phosphate

Holmium species

Ho	Holmium
^{165}Ho	Holmium-165
^{166}Ho	Holmium-166
Ho^{3+}	Holmium 3+ ion
$HoCl^{2+}$	Holmium chloride 2+ ion
$HoCl_2^{+}$	Holmium chloride + ion
$HoCl.6H_2O$	Holmium chloride hexahydrate
$Ho(OH)_{3\ (aq)}$	Aqueous Holmium hydroxide
$Ho(OH)^{2+}$	Holmium hydroxide 2+ ion
$Ho(OH)_2^{+}$	Holmium hydroxide + ion
$Ho(OH)_4^{-}$	Holmium hydroxide - ion
$Ho(OH)_{3\ (s)}$	Solid Holmium hydroxide
$Ho(NO_3)^{2+}$	Holmium nitrate 2+ ion

Other chemical species

^{89}Zr	Zirconium-89
^{89}Sr	Strontium-89
^{111}In	Indium-111
^{166}Er	Erbium-166
^{177}Lu	Lutetium-177
$^{223}RaCl_2$	Radium-223 chloride
CME	Cellulose mixed esters

Cl^-	Chloride ion
DOTA	2,2′,2″,2‴-(1,4,7,10-Tetraazacyclododecane-1,4,7,10-tetrayl)tetraacetic acid
DOTMP	((1,4,7,10-Tetraazacyclododecane-1,4,7,10-tetrayl)tetrakis(methylene))tetraphosphonic acid
DTPA	diethylenetriaminepentaacetic acid
H_3PO_4	Phosphoric acid
HCl	Hydrochloric acid
HEPES	2-[4-(2-hydroxyethyl)piperazin-1-yl]ethanesulfonic acid
HNO_3	Nitric acid
In^{3+}	Indium 3+ ion
$In(OH)_3$	Indium hydroxide
NaOH	Sodium hydroxide
NO_3^-	Nitrate ion
NOTA	2,2′,2″-(1,4,7-triazacyclononane-1,4,7-triyl)triacetic acid
PCL-PEO	Polycaprolactone-block-Polyethylene oxide
PE	Polyethylene
PLA-PEO	Polylactic acid-block-Polyethylene oxide
PP	Polypropylene
PS-PEO	Polystyrene-block-Polyethylene oxide
PB-PEO	Polybutadiene-block-polyethyelene oxide

Units

Bq	Becquerel
kBq	kilo Becquerel
MBq	Mega Becquerel
Bq/ml	Becquerel per milliliter
kBq/ml	kilo Becquerel per milliliter
eV	electronvolt
keV	kilo electronvolt
MeV	Mega electronvolt
keV/mum	kilo electronvolt per micrometer
mg	milligram
mg/ml	milligram per milliliter
ml	milliliter
mul	microliter
m	meter
cm	centimeter
mm	millimeter
mum	micrometer
nm	nanometer
M	molar
mM	millimolar
pM	picomolar
n	neutron
s	second
h	hour

Other symbols and abbreviations

α	alpha
β	beta
γ	gamma
(n, γ)	neutron, γ reaction
CHEAQS	CHemical Equilibria in AQuatic Systems
Cryo-TEM	Cryogenic Transmission Electron Microscopy
EBRT	Electron Beam Radiotherapy
$E_{\beta-,max}$	Maximum beta- emitted energy
EPR	Enhanced Permeability and Retention
FDA	Food and Drug Administration
FTIR	Fourier-Transform Infrared Spectroscopy
ICP-OES	Inductively coupled plasma - optical emission spectrometry
LE	Loading Efficiency
PET	Positron Emission Tomography
PSMA	Prostate specific membrane antigen
RE	Radiolabelling Efficiency
RNT	Radionuclide Therapy
SEC	Size Exclusion Chromatography
SPECT	Single Photon Emission Computed Tomography
WHO	World Health Organizarion

1 Introduction

1.1 Motivation

Cancer is one of the leading causes of death in the world [1]. According to the World Health Organization (WHO), it accounted for nearly ten million deaths in 2020, causing the death of one in six people [1]. This has led many researchers to look for more effective methods to treat cancer, especially attempting to reduce the number of deaths and the severeness of secondary effects that different treatments can cause. The main methods to treat cancer include surgery to remove the tumour if possible, chemotherapy where drugs are used to induce cell apoptosis of the tumour, and radiotherapy, which uses high energy particles to cause cell death [2]. Within radiotherapy, two methods are used for different applications: External Beam Radiation Therapy (EBRT), and Radionuclide Therapy (RNT). The main application of the former is the treatment of local tumours by irradiating a limited area around the tumour with high energy beams [2], while the latter is meant to attack metastases all over the body by the application of beta or alpha emitters, either intravenously or via ingestion [2].

When selecting a radionuclide candidate for RNT, characteristics such as the energy of the radiation emitted, the range of this radiation and the half-life of the radionuclide are considered [2]. These will be discussed in more detail in section 2.1. One promising candidate that is being researched currently is Holmium-166 (^{166}Ho), a lanthanide radioisotope with a short half-life (26.8 h), that emits high energy beta particles (1774.32 keV and 1854.9 keV), as well as gamma (γ) particles [3]. Thanks to its high energy beta emission, it is an effective radionuclide for therapy in large tumours.

Holmium exists in nature as stable Holmium-165 (^{165}Ho), with 100% abundance [4], so its radioactive isotope must be produced by irradiation. There are two main production methods being investigated currently for the production of ^{166}Ho, i.e. via the neutron capture of ^{165}Ho and via the neutron capture of Dysprosium-164 (^{164}Dy) to Dysprosium-166 (^{166}Dy) [3] and the decay of ^{166}Dy to ^{166}Ho. Both methods have their own advantages and disadvantages, but the main advantage of production through the irradiation of ^{164}Dy is the possibility of creating an *in vivo* radionuclide generator. That is, taking advantage of the longer lived but lower energy emitting ^{166}Dy to more effectively deliver ^{166}Ho at the tumour site [5]. The use of an *in vivo* generator is very desirable because of the radiation dose that can be achieved by administering ^{166}Dy rather than ^{166}Ho to a patient. Using an *in vivo* generator, double the radiation dose will be achieved through the same administered dose.

An important consideration in the design of a radiopharmaceutical for use in RNT is the use of a compound or material that will cage the radionuclide, ensuring the specificity of the treatment toward the tumour and reducing side effects [2]. This is usually done through the caging of the radionuclides using a chelator, such as ((1,4,7,10-Tetraazacyclododecane-1,4,7,10-tetrayl)tetrakis(methylene))tetraphosphonic acid (DOTMP) when using ^{166}Ho [3]. However, when designing an *in vivo* generator, chemical differences between the mother and daughter nuclides, as well as the decay of the mother nuclide into the daughter nuclide can cause the release of the radionuclide before accumulating in the tumour, resulting in damage to healthy tissues [5], [6]. Because of this, finding a chelator-free method to encapsulate radionuclides becomes more desirable for the design of the ^{166}Dy/^{166}Ho *in vivo* generator.

A promising chelator-free method to encapsulate radionuclides has already been designed at the Applied Radiation and Isotopes Research team at TU Delft by Liu et al. [7], [8] who successfully radiolabelled polymeric micelles with Indium-111 (^{111}In), Lutetium-177 (^{177}Lu) and Zirconium-89 (^{89}Zr). The mechanism behind this labelling method is quite promising to entrap the radionuclide because the method does not rely on the bonding between the radionuclide and the polymer used to make the micelles. This could lead to a more stable approach to bring radionuclides to the tumour. It is also a fast, simple and highly reproducible method, that has shown high labelling efficiencies with the radionuclides mentioned before.

Based on what was explained above, a promising radiopharmaceutical for cancer treatment could be made by using polymeric micelles to immobilize a ^{166}Dy/^{166}Ho *in vivo* generator, if successfully designed and evaluated.

1.2 Project Scope and Objectives

The main objective of this project is to evaluate whether polymeric micelles can serve as effective carriers for the ^{166}Dy/^{166}Ho *in vivo* generator. To be considered effective nanocarriers, polymeric micelles must perform well in two main characteristics: high radiolabelling efficiency and stability. The former is important so that extremely high activities of the radionuclide are not required during preparation. The latter is essential so that loss of radionuclide is low and will not damage healthy tissues. As studied by Liu et al., the two most effective micelles in the radiolabelling of ^{111}In and ^{177}Lu were those prepared with polycaprolactone-block-polyethylene oxide (PCL-PEO) and polylactic acid-block-polyethylene oxide (PLA-PEO) [7], [8]. Therefore, only these micelles will be evaluated in the current work.

To achieve this goal several objectives are to be pursued or were pursued:

- To determine the loading efficiency of radioactive and non-radioactive Dysprosium in the micelles
- To determine the radiolabelling stability- when challenged with DTPA.
- To understand the mechanism behind the radiolabelling of the micelles.
- To test and tune the mechanism for radiolabelling of micelles with the ^{166}Dy/^{166}Ho *in vivo* generator.

1.3 Outline

The outline of this report is as follows: Chapter 2 will provide all theorical bases required to understand the research performed; Chapter 3 gives the methodology of the experiments; Chapter 4 will show the results and discussion; Chapter 5 summarizes the conclusions made based on all findings and discusses recommendations for the continuation on this research.

2 Theory

2.1 Radionuclide Therapy

Radionuclide therapy is a form of radiation treatment which is unique in that it can selectively apply radiation doses to target cells, while mostly sparing healthy cells [2], [9]–[11]. It lies in between external beam radiation therapy and chemotherapy [2] in that it delivers the radiation directly into the cells, but is delivered in a way that more closely resembles chemotherapy. The main advantage of using RNT instead of EBRT lies in its ability to eliminate metastases in the patient's body, which may not have even been detected yet, as well as the primary tumour [12]. Another main advantage is that radiopharmaceuticals can potentially destroy tumour cells that are adjacent to the tumour but not a part of it, even if the uptake of the radiopharmaceutical is low [12]. Also, because of the selectivity that is at the centre of radionuclide therapy, it causes less side effects to patients.

There have already been two main clinical successes in RNT, that are currently used to treat patients. The first is Novartis's Lutathera®, which is used to treat specific neuroendocrine tumours that are inoperable. These tumours overexpress receptors for the protein somatostatin. Thus, by coupling ^{177}Lu to a somatostatin analogue, DOTA-TATE, which will accumulate in places where it finds the somatostatin receptors [13], the radioactive dose is delivered and cell death is induced. This radiopharmaceutical was approved by regulatory agencies in 2017 in Europe and 2018 in the United states, and has already been administered to more than 9000 gastroenteropancreatic neuroendocrine tumour (GEP-NET) patients in both regions [14]. Another great success is the use of ^{225}Ac-PSMA-617 for the treatment of metastatic castration resistant prostate cancer. By designing a radiopharmaceutical with Prostate specific membrane antigen (PSMA) and coupling it with DOTA, it is possible to cage ^{225}Ac. This leads to a very effective treatment, as ^{225}Ac has higher energy, shorter range and stronger killing effect on tumour cells compared to ^{177}Lu [15]. ^{225}Ac-PSMA-617 is still in the first phase of clinical trials [16] but, if it follows the path of ^{177}Lu-PSMA-617, it will probably be approved, as the first clinical studies show that it is a safe and effective treatment option [15].

RNT relies on the use of radiopharmaceuticals to deliver the radiation dose. Radiopharmaceuticals are usually made of two parts: a radioisotope and a carrier. The carrier is in charge of using the known characteristics and unique features of tumours and the tumour microenvironment to selectively target it. This will ensure that most of the radiopharmaceutical is accumulated at the tumour site [2], [11]. For example, the DOTA-TATE carrier in Lutathera® uses an analogue to a protein whose receptor is overexpressed in the tumour site, somatostatin. Thanks to it, as the radiopharmaceutical transits the body, it will selectively accumulate there, coupled with DOTA, which carries the radioisotope. The radioisotope, meanwhile, is a radioactive isotope, which will emit high energy particles to induce cell death. For example, ^{225}Ac-PSMA-617 uses ^{225}Ac, which emits high energy α radiation in a reaction chain that delivers 4 α particles, 2 β particles and 2 γ photons [15], which readily induces cell death. As such, there are many considerations of importance when selecting each of the parts of the radiopharmaceutical.

Ideal carriers should meet certain requirements to be suitable for use in RNT. First and foremost, it should ensure that most of the radionuclide is not released, since that will increase the radiation dose to healthy tissues, and therefore, increase unwanted side effects. Second, it should be non-toxic, as the carrier itself should not have a pharmacological effect [2]. To ensure this, it is recommended to use carriers that are already approved by regulatory organizations such as the FDA. The carrier should also be resistant to radiation degradation [2], ensuring that it will not be significantly affected by the radionuclide it carries. It should be easily available or easy to prepare [2], and it should not induce an immune response from the body [2]. Examples of carriers will be discussed in section 2.3, specifying their effectiveness for use in the ^{166}Dy/^{166}Ho *in vivo* generator.

Meanwhile, radionuclide selection also requires many considerations, since different radionuclides may be more suitable for different types of tumours and can lead the way to personalized therapy. In general terms, it is imperative to select the radionuclide based on its radiation characteristics, but also the ease at which it can be produced, as well as taking its radionuclidic purity into account [2], [11]. In terms of radiation characteristics, different tumours require different emitters, depending on size. For example, beta (β^-) emitters are effective against larger tumours, since the

range of their emission is longer, whilst alpha (α) emitters are more effective against small tumours [2], [11]. Table 1 shows characteristics of different radionuclides based on decay characteristics, as exsiccated from Dash et al. [2]. As for half-life, short-lived radionuclides are often used to avoid long-lasting side effects in patients. The longest-lived radionuclide that has been used for radiotherapy is Strontium-89 (^{89}Sr), with a half-life of 50 days. An important consideration for half-life is that it must match well with the *in vivo* pharmacokinetics of the carrier. This means that the radionuclide must have a long enough half-life to ensure that sufficient radiation dose is given to the tumour [2].

Table 1. Characteristics of therapeutic radionuclides based on decay characteristics. Adapted from [2]

Characteristic	Beta emitters	Alpha emitters	Auger electron emitters
Emission type	Negatively charged electron	Helium nucleus	Auger and Coster Kronig electrons
Energy	0.05-2.5 Mev	2-10 MeV	10 eV – 10 keV
Range	0.2-15 mm	50-100 µm	10-100 Nanometers
Linear Energy Transfer (keV/µm)	0.2	80-300	4-26
Mechanism	Cross fire effect, half-life and radioactivity dependent, oxygen dependent	Traversed path length in the cell nuclei, oxygen independent	Breaks in DNA Strands when inserted in nuclei ("Bystander" effect), water radiolysis
Requisite	Must be close to target	Must bind to cancer cell	Must incorporate into cell nucleus
Cross fire effect	Yes	No	No
Clinical Application	Some applications are already FDA approved	One application ($^{223}RaCl_2$) is FDA approved	Fully experimental
Suitable for	Large metastases	Small metastases	Small metastases

2.2 ^{166}Ho: A potential candidate for RNT

^{166}Ho has proven to be a promising candidate for RNT [2], [3], [5], [10], [17]. It decays to ^{166}Er through β^- decay. The β^- particles emitted have energies of $E_{\beta,max}$ = 1774.3 keV and 1854.9 keV in a 48.8% and 49.9% yield. It also emits γ rays with an energy of 81 keV. It has a half-life of 26.8 hours [3]. From Table 1, it is possible to see that ^{166}Ho will be useful as a therapeutic radionuclide for large metastases. This is further shown by study made by Johnson and Yanch, which shows that the maximum tissue range of irradiation by ^{166}Ho is 8.7 mm, the average range of irradiation is 2.2 mm and the distance by which 90% of the absorbed dose is imparted to tissues is of 2.1mm [18]. Due to its short half-life, 90% of the administered dose is delivered within 4 days, which represents a relatively higher dose than that administered by other radionuclides that are widely used for RNT [3].

In the past few years, ^{166}Ho has been researched in various studies for RNT with different types of carriers, such as liposomes, microspheres, nanoparticles and antibodies being researched [3]. Carriers that have been proposed include coupling ^{166}Ho to bone seeking agents such as DOTMP [19], [20], complexes such as DOTA [21] and DTPA [22], as well as the use of mesoporous carbon nanoparticles [23]. Some radiopharmaceuticals containing ^{166}Ho have even gone to clinical trials. A notable example of this are Quirem microspheres, that have completed several clinical trials, as shown in clinicaltrials.gov [24]–[27]. Quirem microspheres are Poly-L-Lactic acid microspheres, that use a solvent evaporation method to encapsulate ^{165}Ho and then are irradiated to obtain ^{166}Ho [28]. These microspheres are used as a method of radioembolization on hepatocellular carcinoma patients. They are inserted to the tumour through a catheter in the hepatic artery, which primarily irrigates cancer cells [29], therefore delivering radiation selectively to hepatic tumours.

Although the use of ^{166}Ho is already well researched, due to its short half-life of 26.8 hours it provides a somewhat too short treatment. A way to increase the radiation dose delivered is the use of the Dysprosium-166/Holmium-166 (^{166}Dy/^{166}Ho) *in vivo* generator. This is, delivering a therapeutic isotope through the decay of its longer lived mother nuclide [5]. In this case, it will constitute the creation of a radiopharmaceutical containing ^{166}Dy, which will deliver the

radiation dose of ^{166}Ho to the desired tissues. The main advantage of the ^{166}Dy/Ho *in vivo* generator is that it is possible to achieve more than double the dose of radiation per administered activity than when administering ^{166}Ho directly. ^{166}Dy is also a β^- emitter with a longer lived half-life of 81.6 hours and emitting lower β^- energy (400 and 481 keV compared to the 1774.32 keV and 1854.9 keV emitted by ^{166}Ho).

^{166}Dy and ^{166}Ho are in radioactive equilibrium with each other. When a daughter nuclide is formed at the same rate as it is decaying, so the ratio of masses N_2/N_1 is constant, it is considered to be in equilibrium. It is important to distinguish radioactive equilibrium from chemical and thermodynamic equilibrium in that it is not reversible. For example, ^{166}Ho cannot decay into ^{166}Dy, and it does not represent a stationary state [30]. There are two types of radioactive equilibrium, secular and transient, the one present in the ^{166}Dy/Ho *in vivo* generator is transient equilibrium, as the half-life of ^{166}Dy is only around three times the half-life of ^{166}Ho. In transient equilibrium, the activity of the daughter nuclide is higher than that of its mother, defined by $\frac{A_2}{A_1} = 1 - \frac{t_{1/2}(2)}{t_{1/2}(1)}$. Also, the half-life of the daughter radionuclide appears to become equal to that of its mother, because of its rate of decay being equal to its rate of formation. This is what allows the ^{166}Dy/^{166}Ho *in vivo* generator to deliver twice the dose when compared to the administration of ^{166}Ho alone.

The *in vivo* generator works as follows: Before the conjugation of the *in vivo* generation system, usually the mother nuclide (^{166}Dy in this case) is isolated and encapsulated. This way, as sub-equilibrium amounts of ^{166}Ho are in circulation, while ^{166}Dy emits much lower energy when decaying, there is a reduced radiation dose to non-target tissues [5]. As time goes by, and the radiopharmaceutical accumulates in the tumour site, the therapeutic dose is generated via the decay of ^{166}Ho, which is now present by the decay of ^{166}Dy [5], [31].

2.3 Methods to carry radionuclides in the body

2.3.1 Binding radionuclides to chelating agents

As mentioned in section 2.2, the design of a radiopharmaceutical requires both the selection of a suitable radionuclide, as well as a carrier for the radionuclide. Now that the suitable radionuclide has been selected, as well as the use of the ^{166}Dy/^{166}Ho *in vivo* generator, the next exploration will discuss carriers. As discussed before, the carrier is responsible of using tumour-specific characteristics to selectively accumulate in the tumour. A very important characteristic that every carrier must achieve is the safe entrapment of radionuclides. For this, most RNT carriers use a chelating agent [3]. Chelating agents are ligands that can form two or more coordinate covalent bonds with a metal ion [34]. The radionuclide will not be released by the chelating agent unless this bond is broken or that the dissociation rate of the complex is high. Many chelating agents have been designed successfully for their use in RNT. Some examples of these can be seen in Figure 1.

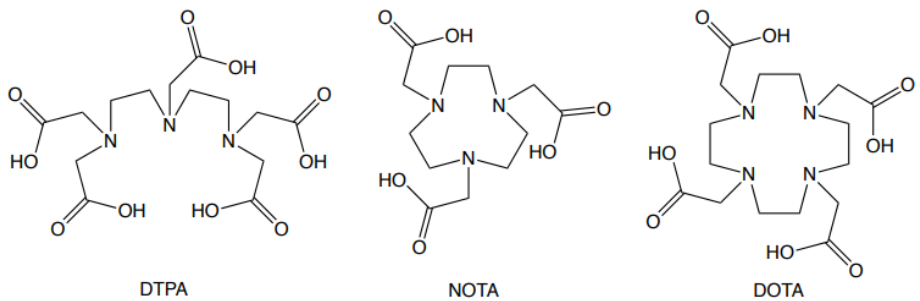

Figure 1. Common chelating agents used with radionuclides. Taken from [35]

As mentioned before, there are various radiopharmaceuticals that successfully use chelating agents as part of the carrier for radionuclides in RNT. In fact, this is used by both clinical successes mentioned in section 2.1. However, the

use of chelating agents presents issues when it comes to the design of radiopharmaceuticals that carry *in vivo* generators. If the mother and daughter nuclides are very different chemically, the decay of the mother to the daughter will probably lead to the premature release of the daughter [5] [6]. This is the main challenge faced when making an *in vivo* generator for α emitters, that usually undergo decay through a decay chain that happens during a short time, and the daughter nuclide will have a small chance of binding back to the same chelator even if that is not the case, as they will have moved away from the chelator[36]. This is not expected to be an issue for the ^{166}Dy/^{166}Ho generator, since the two radionuclides share most chemical characteristics.

Nevertheless, the unexpected release of ^{166}Ho from chelators has presented itself as a very significant issue when designing a carrier for the ^{166}Dy/^{166}Ho *in vivo* generator. In their work on *in vivo* generators, Zeevart et al. sought to understand the caging of *in vivo* generators, and the reasoning behind the unexpected release of daughter nuclides from chelating agents [36], [37]. In the preparation and elution of a ^{166}Dy/^{166}Ho *in vivo* generator conjugated to DOTA, they found that around 72% of the Dy was released from DOTA when decaying to Ho, which was unexpected from their original calculations [37]. They proposed that the reasoning behind this release was the decay from ^{166}Dy to ^{166}Ho*, which led to the de-excitation of ^{166}Ho* to ^{166}Ho through the emission of Auger Electrons. As many electrons can be lost from the atom during the Auger emission process, the now highly charged ion becomes an electron sink, seeking to take surrounding electrons. The only place that the ion can take electrons from is the chelator, and if the electrons taken were making the coordinate covalent bonds that characterize chelators, the molecule will break, and ^{166}Ho will be released prematurely [36], [37]. This was corroborated by the total emission of Auger electrons by Ho, which matched the 72% of metal released when conjugating DOTA with ^{166}Dy to make the ^{166}Dy/Ho generator.

Based on the issue explained above, chelator-free methods are being sought to carry the *in vivo* generator itself. One such option is the use of polymeric micelles, whose advantages and functioning will be discussed in section 2.3.2.

2.3.2 Polymeric micelles

Polymeric micelles are a form of nanostructures formed by the self-assembly of amphiphilic block copolymers [38]. Many envision the formation of micelles as “core-shell” structures with a water-free core and an outer shell composed of hydrophilic blocks [39], [40]. These structures are formed due to the presence of two antagonistic parts in the molecule: one hydrophobic, one hydrophilic, seeking to the surface area of contact between the liquid and the hydrophilic part of the molecule while at the same time minimizing the surface area of contact between the hydrophobic part of the molecule and the liquid. This leads to particular characteristics in solution, such as their ability to adsorb substances at the interface [41]. These structures have a wide variety of geometries [41], such as spherical and cylindrical, among others. Figure 2 shows a schematic that illustrates the formation of polymeric micelles.

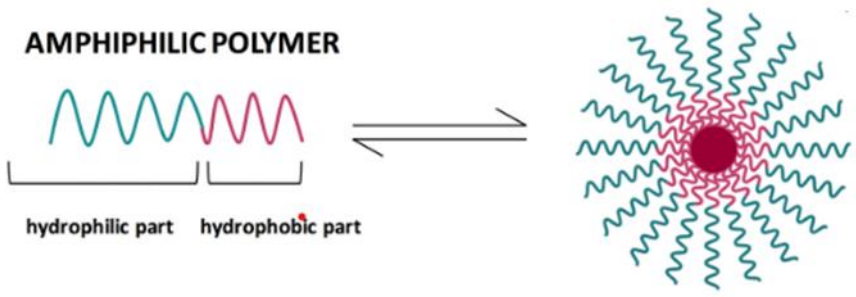

Figure 2. Schematic representation showing the formation of a polymeric micelle. Adapted from [42].

A big advantage found when designing micelles for different applications is how easily they can be tuned. Morphological changes in micelles can be achieved by changing different parts of the micelle production process, with changes such as using a different block copolymer system and the size of the polymer chains having an effect on the resulting micelles, their hydrophobicity, their ability to encapsulate substances, release kinetics and micelle stability [39]. However, preparation methods are often flexible, and there is a high degree of control over the polymer structures [41].

Polymeric micelles are already being used for different types of cancer therapy. They are often very easy to make, and it is possible to encapsulate water-insoluble drugs as well as radionuclides within them [7]. The reason why they are very promising for the controlled delivery of pharmaceuticals for cancer treatment is their reliance on the Enhanced Permeability and Retention (EPR) effect, which differentiates tumour vasculature from other tissue vasculature and allows for the permeation of macromolecular drugs such as liposomes, micelles, and other nanoparticles into the tumour [43]. They have already even been used to encapsulate radionuclides such as an ^{111}In-tropolone complex in polystyrene-block-polyethylene oxide micelles [44], among others.

A common concern when designing drug targeting molecules is the rapid recognition of these molecules by the reticuloendothelial system, which will subsequently eliminate them via the kidneys or liver before they have reached their target [40]. However, the use of polyethylene oxide (PEO) in many cases has proven to decrease the uptake by this system, endowing drug delivery systems with a sort of stealth character [40], [45]. Therefore, drug delivery systems containing PEO present longer circulation times and, coupled with the EPR effect, have been found to be promising in cancer treatment.

Polymeric micelles are also useful in the search for a chelator-free method to carry radionuclides, as evidenced in the research made by Liu [7]. In her doctorate studies, Liu designed a method by which ^{177}Lu, ^{111}In and ^{89}Zr were successfully encapsulated into four different types of micelles: poly-ε-caprolactone-block-poly ethylene oxide (PCL-PEO), poly lactic acid-block-poly ethylene oxide (PLA-PEO), poly styrene-block-poly ethylene oxide (PS-PEO) and poly butadiene-block-poly ethylene oxide (PB-PEO); and began to understand the process by which the radiolabelling may occur, further explained in section 2.3.3 [7], [8]. From her findings, the two polymers that were most successful in the radiolabelling were those made with PCL-PEO and PLA-PEO polymers. This was explained through the possible formation of hydrogen bonds between the carbonyl ends in PCL and PLA. These lead to more water molecules coming in contact with the micelle core [39], [46], which might be essential to the method for radiolabelling micelles used, as it is diffusion based. The proposed mechanism is further explained in section 2.3.3.

2.3.3 Mechanism of radiolabelling polymer micelles

This section seeks to give an explanation about how the method used by Liu et al., and this report, to radiolabel micelles without the need of a chelator intermediate. In the manuscript “Efficient radiolabelling of block copolymer micelles through radiometal salt precipitation for theranostic applications”, Liu et al. [8] used FTIR, cryo-TEM and loading efficiency studies to understand the interactions formed between PCL-PEO micelles and different metal ions, especially In^{3+}. Through FTIR results, it was possible to conclude that the encapsulation of metal ions was not caused by the formation of coordination bonds between the polycaprolactone and the metal ions. Meanwhile, through the latter two studies, it was possible to observe the appearance of black dots forming inside the micelles (as seen in Figure 3) with an increase of time. Aided by a simulation using CHEAQs, a programme that calculates the speciation of systems that contain specific cations and anions or other ligands [47], it was possible to determine that this black dot formation is probably attributed to the formation and precipitation of $In(OH)_3$.

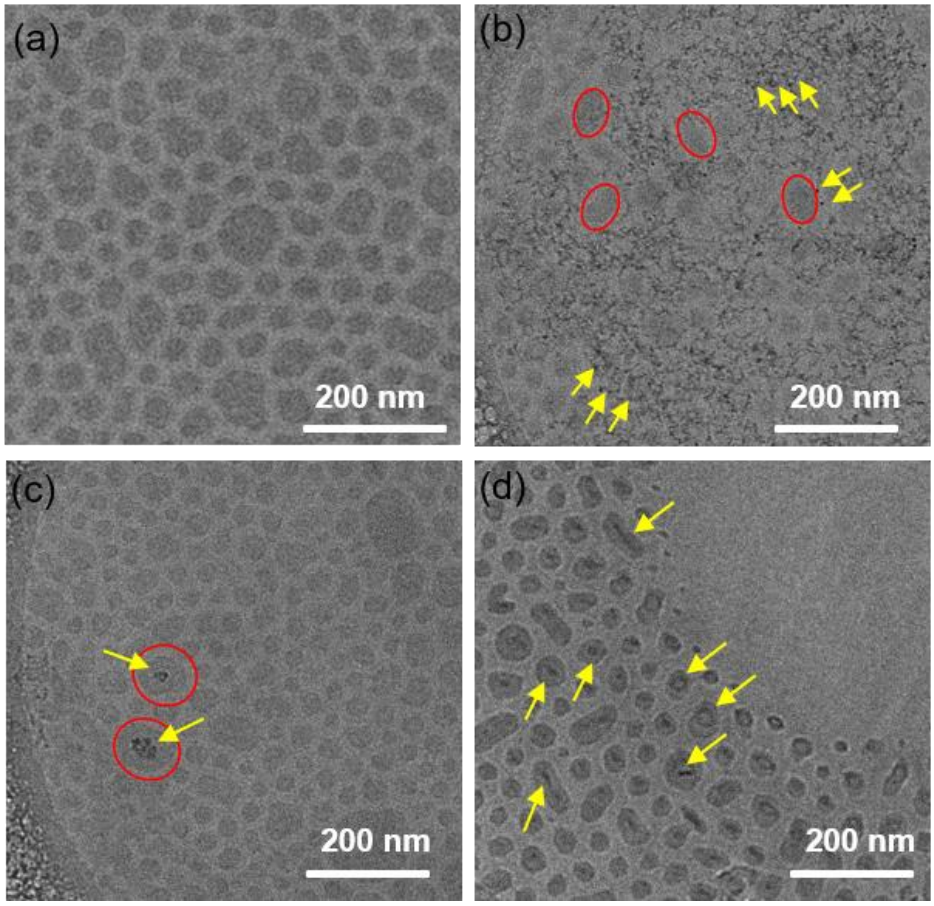

Figure 3. Cryo-TEM images of a) empty PCL-10000 micelles, and after b) 2 min, c) 10 min, and d) 30 min of adding In ions. Taken from [7]

Based on the experimental findings explained above, Liu et al. proposed that the mechanism for loading micelles with metal ions such as In^{3+} consists of the following steps:

1. Upon the addition of metal ions into the micelle solution, aqueous metal hydroxides are spontaneously formed.
2. The metal hydroxide will diffuse into micelles, entering the micelle core.
3. Upon accumulation of the metal hydroxides within the micelles, the concentration will rise until a point where the metal hydroxides will precipitate within the micelle core, and will be thus stably encapsulated.

Although, as mentioned by Liu et al., the driving force behind the accumulation of the In species in the core of the micelles is unknown, it is possible to define some parameters that may have a significant effect on the loading of the micelles with metal ions and the stability of the encapsulated material:

1. To achieve radiolabelling, metal hydroxides must diffuse into the micelles. Therefore, the kinetics behind the loading are both concentration and time-based. For the former, the main challenge is probably achieving the right concentration inside the micelle core to achieve precipitation, since free metal ions are capable of diffusing out of the micelle core, leading to micelles that may have a high radiolabelling efficiency but low stability.
2. For a stable encapsulation of metal ions, precipitation must occur within the micelle core. In systems that do not achieve precipitation, it might be possible to add ligands that induce the precipitation of micelles, such as phosphate ions, which are known to interact with lanthanides to form insoluble salts [48]. A possible challenge here may be that it is not known what happens if the metals precipitate prematurely. That is, if the metals would still be encapsulated if they precipitate outside of the core of the micelles.

3 Materials and Methods

3.1 Materials

3.1.1 Chemicals

Every chemical used in this work is listed in Table 2 below.

Table 2. Chemicals used, with CAS number, and supplier.

Chemical	CAS number	Supplier
Acetonitrile	75-05-8	Honeywell
Chloroform	67-66-3	VWR Chemicals
DTPA	67-43-6	Sigma Aldrich
$Dy(NO_3)_3 \cdot 5H_2O$	10031-49-9	Alfa Aesar
Dy2O3	10031-49-9	Sigma Aldrich
$DyCl_3 \cdot 6H_2O$	10025-74-8	Sigma Aldrich
Dysprosium ICP standard	10025-74-8	Merck
HCl	7732-18-5 (68%) 7647-01-0 (32%)	Merck
HEPES	7365-45-9	Sigma Aldrich
HNO3	7732-18-5 (<35%) 7697-37-2 (>65%)	Honeywell
$HoCl_3 \cdot 6H_2O$	14914-84-2	Sigma Aldrich
Holmium ICP standard	10025-74-8	Merck
PCL-PEO (2000-2800)	NA	Polymer Source, inc.
PLA-PEO (5000-6500)	NA	Polymer Source, inc.
Sephadex G-25 medium	9041-35-4	Sigma Aldrich

3.1.2 Consumables

The most relevant consumables used in this work can be found in Table 3.

Table 3. Consumable equipment used to perform all experiments, with supplier.

Consumable	Supplier
Amicon Ultra-4 centrifugal filters, ultracell - 10k	Merck
Sample vials 4ml with caps	Rotilabo
Snapcap vial 20 ml	VWR
Syringe filter CME, unsteril, pore size 220 nm, nominal diameter 25 mm	Rotilabo
Syringe filter CME, unsteril, pore size 450 nm, nominal diameter 25 mm	Rotilabo
Tube 15 ml, PP	Sarstedt
Tube 50 ml, PP	Sarstedt

3.1.3 Equipment

Table 4. All electronic equipment used for sample preparation and measurement, specifying supplier and model.

Equipment	Supplier	Model	Measurement/ Preparation
Centrifuge	Thermo	Jouan CR4i	Preparation
ICP-OES	Perkin Elmer	Optima 8000	Measurement
Small Ultrasonic bath	Branson	200	Preparation
Big Ultrasonic bath	Branson	5800	Preparation
Wallac Gamma Counter	Perkin Elmer	Wizard$^{2}{}_{TM}$3", 2480 Automatic Gamma Counter	Measurement

3.2 Methods

3.2.1 Speciation analysis using CHEAQs

Three different types of speciation analysis were performed using the Chemical Equilibria in Aquatic Systems (CHEAQS) software [47] for both Dysprosium and Holmium. The first set of simulations sought to observe the effect of changing the concentration of metal ions in the system, while keeping all other conditions equal. The constant conditions were: a pH of 7 and, in the case of chlorides, an anion concentration of 0.1 mM. In the case of nitrates, an increasing metal concentration also led to an increasing nitrate concentration. The second set of simulations sought to observe the effect pH had on the system, while keeping metal ion and anion concentrations constant. For nitrates, metal ion concentrations were equivalent to 0.084 mM for Dysprosium, and 50 kBq, or $1.18 \times 10^{-11} M$ for Holmium, while nitrate concentration was kept constant at 0.252 mM. For chlorides, metal ion concentrations were 0.074 mM for Dysprosium and 50 kBq, or $1.18 \times 10^{-11} M$ for Holmium, and chloride concentration was kept constant at 0.1 mM. The final set of simulations sought to observe the changes in speciation when adding phosphate ions into the system. For this, pH was kept at 7, Dysprosium concentration was kept at 0.084 mM and 0.074 mM for nitrates and chlorides respectively, and Holmium concentration was equivalent to 50 kBq, or and $1.18 \times 10^{-11}\ M$, while nitrate and chloride concentrations were kept at 0.252 mM and 0.1 mM respectively.

3.2.2 Synthesis

3.2.2.1 Synthesis of polymeric micelles

Polymeric micelles were synthesized using a solvent evaporation method. For PCL-PEO micelles, 20 mg polymer was dissolved in 200 µl chloroform using a sonication bath. This solution was added dropwise to 2.3 ml water and left stirring overnight, partially covered to allow for chloroform evaporation. After the solvent evaporation was completed, micelle solution was passed through a 220 nm cut off CME filter, and 20 mM HEPES solution (pH 7.4) was added to the micelle solution in a ratio of 1:1.

For PLA-PEO micelles, 20 mg polymer was dissolved into 1 ml acetonitrile using a sonication bath. This solution was added dropwise to 4 ml water and left stirring overnight, partially covered to allow acetonitrile evaporation. After the solvent evaporation was completed, the micelle solution was passed through a 450 nm cut off CME filter, and 20 mM HEPES solution (pH 7.4) was added in a proportion of 1:1.

3.2.2.2 Loading micelles with non-radioactive Dy^{3+}/Ho^{3+}

To load micelles with non radioactive Dy^{3+} and Ho^{3+} ions, solutions of 10 mM $DyCl_3 \cdot 5H_20$ and $HoCl_3 \cdot 6H_20$ in HCl (pH 2) were prepared using sonication. Then, different volumes of the metal chloride solutions were added to obtain a total metal concentration of 0.1 mM in the micelle solution, with desired proportions as shown in Table 5.. This was left stirring for one hour and a Size Exclusion Chromatography (SEC) column was applied using HCl (pH 2) as an eluent. For this, columns were prepared in-house using Sephadex G-25 medium gel. SEC was used to separate the loaded

micelles from free Ho and Dy ions remaining in the micelle solution. Every 1ml of liquid was collected as a fraction and the micelles were obtained in the 8th-13th fractions. In total, around 6 ml of micelle solution was obtained.

Table 5. concentration of Dy and Ho present in the five types of non-active experiments.

Name of experiment	Concentration of Dy^{3+} in solution (mM)	Concentration of Ho^{3+} in solution (mM)
100% Dy 0% Ho	0.1	0
75% Dy 25% Ho	0.075	0.025
50% Dy 50% Ho	0.05	0.05
25% Dy 75% Ho	0.025	0.075
0% Dy 100% Ho	0	0.1

3.2.2.3 Radiolabelling micelles with $^{166}Dy/^{166}Ho$

Two types of Dy were irradiated in-house to perform the experiments: for experiments with lower activity (1-5 kBq/ml), 15 mg of $Dy(NO_3)_3$ was irradiated in a PE (polyethylene) rabbit for 10 hours in the HOR (Hoger Onderwijs reactor) of the TU Delft (BP3, thermal neutron flux of $4.66 \times 10^{16} s^{-1} \cdot m^{-2}$ and epithermal neutron flux of $8.8 \times 10^{14}\ s^{-1} \cdot m^{-2}$), and cooled for 48 hours before opening it. The activity obtained was around 1MBq, which was dissolved in 5 ml water and small volumes were used for the experiments. For experiments with higher activity (10-50 kBq/ml), 5 mg of Dy_2O_3 was put into a quartz tube and irradiated for 10 hours (SmallBeBe, thermal neutron flux of $4.09 \times 10^{17} s^{-1} \cdot m^{-2}$ and epithermal neutron flux of $3.71 \times 10^{16}\ s^{-1} \cdot m^{-2}$) and cooled for 48 hours before opening. The activity obtained was around 20 MBq, which was dissolved in 1 ml HCl (1M, pH=0), and then neutralized using small volumes of 1M NaOH, to obtain a final pH of 3-4, which was used for radiolabelling (Appendix D–1 explains the decision behind neutralizing the activity source).

To radiolabel the micelles with $^{166}Dy/^{166}Ho$, 1kBq, 5kBq or 10 kBq activity was added per ml of micelle solution (Concentration = 0.708 pM, 3.54 pM and 7.08 pM). The solution was stirred for 30 minutes to complete the process. After this, the activity present in the vials was measured using the Wallac gamma counter and then size exclusion chromatography was performed, this time using HEPES buffer (10 mM, pH 7.4) as an eluent. Again, micelles were collected in the 8th to 13th fractions. The activity for all fractions collected was measured again using the Wallac gamma counter.

3.2.2.4 Radiolabelling micelles with $^{166}Dy/Ho$ with addition of phosphates

Two types of experiments were made to evaluate the effect of adding phosphates during the radiolabelling process. In the first type of experiment, the labelling process was performed as explained in section 3.2.2.3, but small amounts of H_3PO_4 0.04 mM (to reach 10^{-6}M and 10^{-7}M in smaller activity experiments and $3*10^{-8}$ M and 10^{-7}M in higher activity experiments) were added immediately before the addition of $^{166}Dy/Ho$. In the second type of experiment, the labelling process was performed as explained in section 3.2.2.3, but small amounts (to reach 10^{-6}M and 10^{-7}M in smaller activity experiments and $3*10^{-8}$ M and 10^{-7}M in higher activity experiments) of H_3PO_4 were added after mixing the micelle solution with $^{166}Dy/^{166}Ho$ for 30 min, and the new mixture was mixed for another 30 min before measuring activity and performing the size exclusion chromatography.

3.2.3 Characterization

3.2.3.1 Preparation of loaded micelles for evaluation using ICP-OES

The loading efficiency of non radioactive samples was measured using an ICP-OES. To prepare samples for the ICP-OES, loading was performed as explained in section 3.2.2.2, which resulted in 6ml of micelle solution obtained after performing SEC. This solution was concentrated to 1ml using centrifuge filters. Then, 1ml aqua regia was added to the 1ml micelle solution, followed by ultra sonication at 50°C during 4-6 hours to destroy the micellar structure,

leaving ions free in the solution. Then, 5ml Milli-Q water were added to the digested micelle solution, leaving samples ready for ICP.

3.2.3.2 Loading/radiolabelling efficiency

To calculate the loading efficiency (LE), Eq. 1 was used:

$$Loading\ efficiency\ (\%) = \frac{concentration\ measured\ by\ ICP}{concentration\ added\ to\ micelles} \times 100 \qquad \textit{Eq. 1}$$

To calculate the radiolabelling efficiency (RE), Eq. 2 was used:

$$Radiolabelling\ efficiency\ (\%) = \frac{Activity\ present\ in\ fractions\ containing\ micelles}{Activity\ added\ to\ micelle\ solution} \times 100 \qquad \textit{Eq. 2}$$

Decay was accounted for in both values of activity in Eq. 2.

3.2.3.3 Stability tests using DTPA

The radiolabelling stability was determined using 100 µl of DTPA solution (11 mM DTPA in 10 mM HEPES solution), that was added to each ml of radiolabelled micelle solution. This solution was left at room temperature for 24 hours. After 24 hours, size exclusion chromatography was performed, using 10 mM HEPES as eluent. In the DTPA challenge tests, radiolabelled micelles were collected in the 7th to 13th fractions, DTPA chelated ions were collected in the 14th to 17th fractions and free ions were collected in the 18th to 20th fractions. After performing the size exclusion chromatography, activity present in the vials was measured using the Wallac gamma counter, and the retention percentage in both micelles and DTPA fractions was calculated as explained in Eq. 3 and Eq. 4.

$$Retention\ in\ micelles\ (\%) = \frac{Activity\ present\ in\ fractions\ containing\ micelles}{Activity\ present\ in\ labelled\ micelles\ before\ adding\ DTPA} \times 100 \qquad \textit{Eq. 3}$$

$$Retention\ in\ DTPA\ (\%) = \frac{Activity\ present\ in\ fractions\ containing\ DTPA-ion\ complex}{Activity\ present\ in\ labelled\ micelles\ before\ adding\ DTPA} \times 100 \qquad \textit{Eq. 4}$$

Decay was accounted for in all values of activity in Eq. 3 and Eq. 4 using the decay law, by keeping track of the time passed between radiolabelling and measuring and calculating what the activity would be at the time when radiolabelling began.

4 Results and Discussion

4.1 Loading micelles with non-radioactive Dy/Ho

The first set of experiments performed was a proof of concept to ensure that it was possible to encapsulate Dy and Ho ions in both PCL and PLA micelles. This set of experiments was performed with non-active Dy and Ho, to be able to control the amount of Dy and Ho added. One of the objectives of this set of experiments was to see if the loading efficiency would be affected by the loading of both Dy and Ho at different concentrations. This was done to see if there was any preference in the loading, although this is not be expected due to the chemical similarity of both lanthanides. These results are shown in Figure 4.

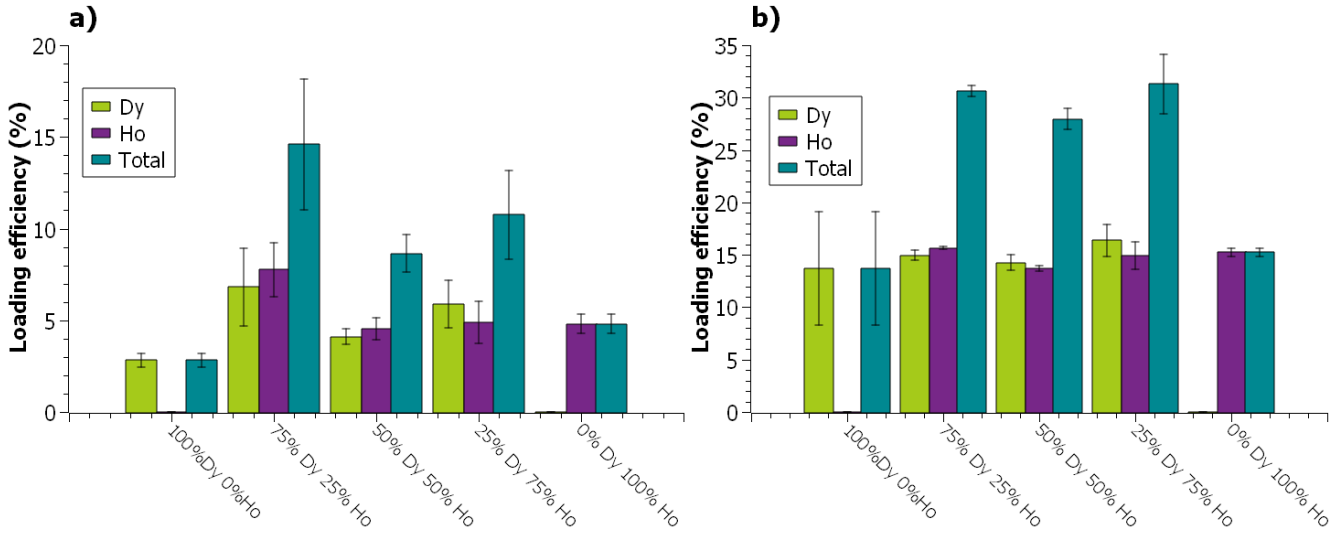

Figure 4. Loading efficiency of Dy and Ho when adding different proportional concentrations of Dy and Ho ions as determined by ICP-OES on a) PCL-PEO, and b) PLA-PEO micelles. (total metal concentration:0.1 mM , polymer concentration: 4.3 mg/ml for PEO-PCL micelles and 2.5 mg/ml for PEO-PLA micelles in 10 mM HEPES buffer with pH of 7.4, loading time: 1 hour, standard error based on 3 repeat experiments).

As can be seen in Figure 4, this first attempt of loading Dy and Ho was successful, and no experiments showed a preference for one of the metals. Although these results were promising since they imply that both metals could be encapsulated, the loading efficiency was low i.e. the maximum achieved was around 30 ± 2% when tested in PLA-PEO micelles.

The next test performed was a test where the total metal ion concentration was increased from 0.1 to 0.2 mM. These results can be seen in Figure 5.

As can be seen from Figure 5, the effect of increasing the total metal concentration in the micelle solution mostly resulted in an increase in the standard deviation. Due to the high standard deviation it cannot be really concluded if higher concentration led to lower radiolabelling efficiency. The increase in experimental uncertainty might be caused by the premature precipitation of metal hydroxides, which do not diffuse as readily into the micelles as their soluble counterparts, or hydroxide ions (such as $Dy(OH)^{2+}$, $Dy(OH)_2^{+}$, $Dy(OH)_4^{-}$ $Ho(OH)^{2+}$, $Ho(OH)_2^{+}$ and $Ho(OH)_4^{-}$), making the loading process much more stochastic by nature.

It is important to note that the experiments performed were an exaggerated version of reality, since the concentration of ^{166}Ho present in radioactive experiments is never expected to be as high as even 25% of the concentration of Dysprosium in the micelle solution. When a $^{166}Dy/^{166}Ho$ generator will be constructed, the amount of generated ^{166}Ho will be very tiny, in the order of pM or nM. As such, although Dy concentrations in radioactive studies will be in the same magnitude as the non-radioactive studies, this will not be the case in Ho, where the concentrations will be in the pM magnitude. Based on this, it is expected that, when radiolabelling micelles, results will be similar to the 100% Dy, 0% Ho case. Anyhow, these higher concentrations were chosen to also make sure that Ho can be properly detected using ICP-OES.

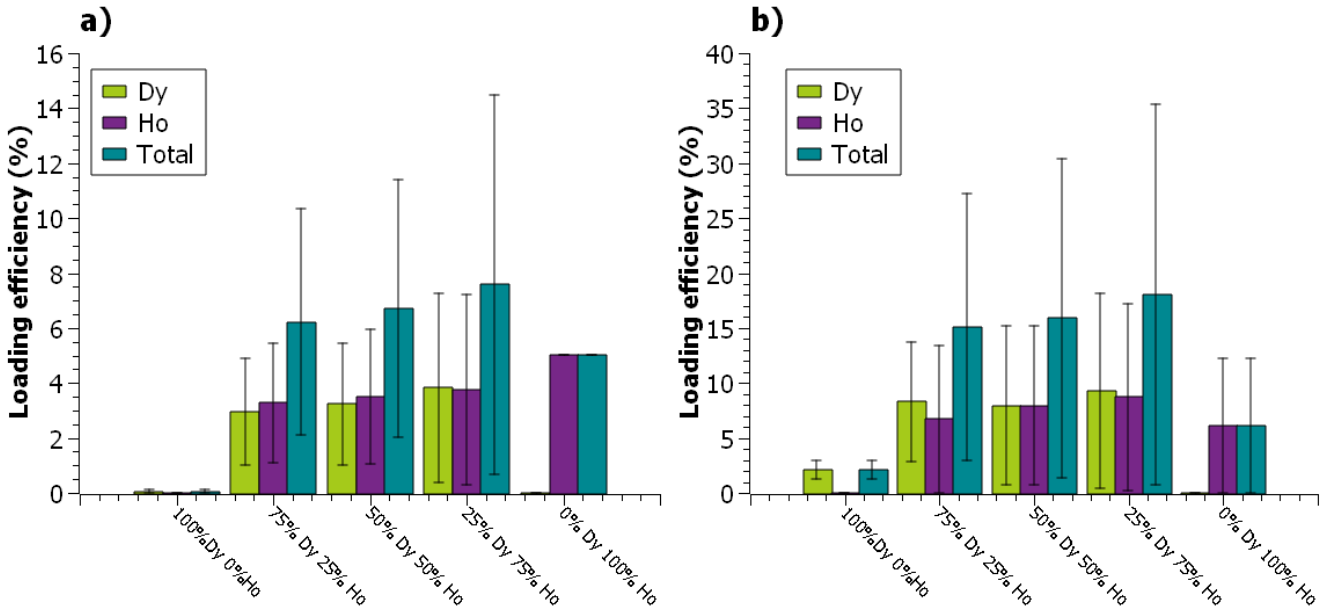

Figure 5. Loading efficiency of Dy and Ho when adding different proportional concentrations of Dy and Ho ions as determined by ICP-OES on a) PCL-PEO, and b) PLA-PEO micelles. (total metal concentration:0.2 mM , polymer concentration: 4.3 mg/ml for PEO-PCL micelles and 2.5 mg/ml for PEO-PLA micelles in 10 mM HEPES buffer with pH of 7.4, loading time: 1 hour, standard error based on 3 repeat experiments)

Since the results were already promising, a decision was made to perform a speciation analysis, which potentially could explain the results obtained with the non-radioactive experiments and would also show if radioactive experiments would also be promising.

4.2 Speciation analysis for Dy and Ho.

Speciation calculations were performed for both $Dy(NO_3)_3$ and Dy_2O_3 since both were used in the radiolabelling studies when applying different radioactivity levels. In the case of Dy_2O_3 HCl was used to dissolve the sample, and thus Cl ions were included in the speciation. Section 4.2.1 shows the speciation analysis made as a function of varying metal ion concentrations, while section 4.2.2 shows the speciation analysis made as a function of pH.

4.2.1 Varying metal ion concentration

Figure 6 shows the speciation of Dy ions and Ho ions as a function of metal nitrate concentration, when pH is kept constant. The first observation that can be made here is that Dy and Ho behave very similarly in their speciation. This was expected, due to their chemical similarity. Second, it is possible to observe that the dominant species throughout the simulation are the free Dy^{3+} and Ho^{3+} ions, although this changes after a concentration of around 10 µM, where solid metal hydroxide precipitates become the dominant species. At lower concentrations, the second most dominant species is the metal hydroxide cation ($Dy(OH)^{2+}$ and $Ho(OH)^{2+}$ respectively).

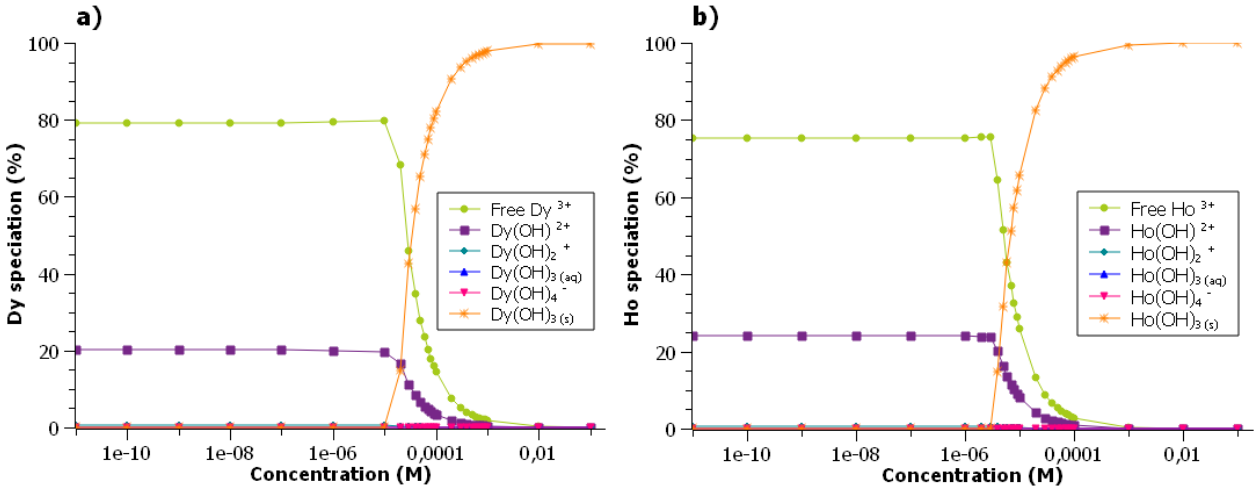

Figure 6. The speciation of a) $Dy(NO_3)_3$ in water at equilibrium as a function of concentration (pH = 7). The speciation of b) $Ho(NO_3)_3$ in water at equilibrium as a function of conentration (pH = 7). These figures were based on data calculated by CHEAQS. For additional information, check Appendix B.

Figure 7 shows the speciation of Dy and Ho ions as a function of metal concentration in an environment that contains chlorides.

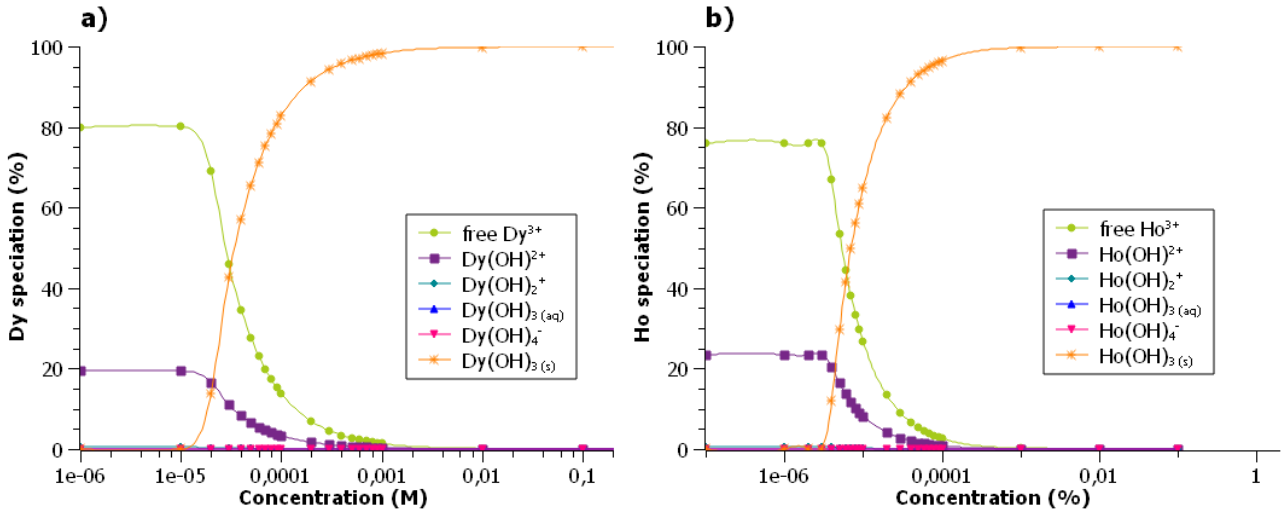

Figure 7. The speciation of a) Dy ions in water at equilibrium as a function of concentration (pH = 7, Cl^- concentration = 0.1 mM). The speciation of b) Ho ions in water at equilibrium as a function of conentration (pH = 7, Cl^- concentration = 0.1 mM). These figures were data calculated by CHEAQS. For additional information, check Appendix B.

As mentioned before, the expectation was that the performance of both radioactive sources would not be very different. This expectation was proven to be correct by Figure 6 and Figure 7, which look almost identical. Therefore, it is expected that the performance of both Dysprosium-166 sources should perform similarly at similar concentrations.

As discussed in section 2.3.3, the mechanism behind radiolabelling micelles is expected to be driven by diffusion and precipitation and based on the speciation analysis performed, this is more specifically caused by the formation of metal hydroxides. To ensure that the metals are caged inside the micelles, inducing the precipitation of solid metal hydroxides is required within the micelles, which occurs when the metal concentration surpasses 10^{-5} M as shown in Figure 6 and Figure 7. However, if precipitation occurs outside of the micelles, the solid precipitates will not as readily diffuse into the micelle's core as their aqueous counterparts. This is supported by the findings shown in Figure 4 and Figure 5, where experiments were performed at 0.1 mM and 0.2 mM respectively. At these concentrations, from the speciation, solid precipitates are the dominant species, especially at 0.2 mM, where almost 100% of the metal has spontaneously precipitated. The results shown in Figure 5 b) have a maximum loading efficiency of 18 ± 17%, and all results present very large standard deviations. Meanwhile, when the metal concentration is decreased to 0.1 mM, the

standard deviation is reduced and the loading is almost doubled, with the maximum loading becoming 31 ± 3%. At 0.1 mM, although the solid precipitate is dominant, there are still free Dy^{3+} ions as well as $Dy(OH)^{2+}$ available to diffuse into the micelle core. This supports the theory that, if all of the metal has precipitated, loading becomes erratic and difficult, and their dominance hinders the ability to load micelles.

4.2.2 Varying pH

Figure 8 shows the speciation of Dy and Ho ions as a function of pH in an environment containing nitrates at fixed metal concentration. Because of the different concentrations expected to be present for Dy and Ho, their speciation differs here. These results also show that increasing the pH does lead to more hydroxides being formed, as expected, but they are positively charged i.e. $Dy(OH)^{2+}$ and $Ho(OH)^{2+}$ respectively. However, this occurs at different pH values for Dy and Ho: the positively charged ions become dominant for Dy at a pH of 10, while the same happens in Ho at a pH of 8. Meanwhile, at basic conditions, the dominant species are the negatively charged species $Dy(OH)_4^-$ and $Ho(OH)_4^-$ respectively. At the expected experimental conditions, that involve a pH of 7.4, the dominant species is the positively charged metal hydroxides in the case of Ho, and free Dy^{3+} ions in the case of Dy. However, positively charged metal hydroxides are the second dominant species in the case of Dy, where almost 2% of the Dy speciates to this ion. It is also important to note that based on Figure 6, it was expected that part of the Dy should speciate into the solid hydroxide form. However, due to limitations of the CHEAQS software, this was not the case, as the software could not find equilibrium when precipitates were included in the pH study (equilibrium could not be found leading to the programs iterating continuously). From Figure 6, we can conclude Dy speciation will likely be around 4% $Dy(OH)^{2+}$ ions and around 79% solid Dysprosium hydroxide.

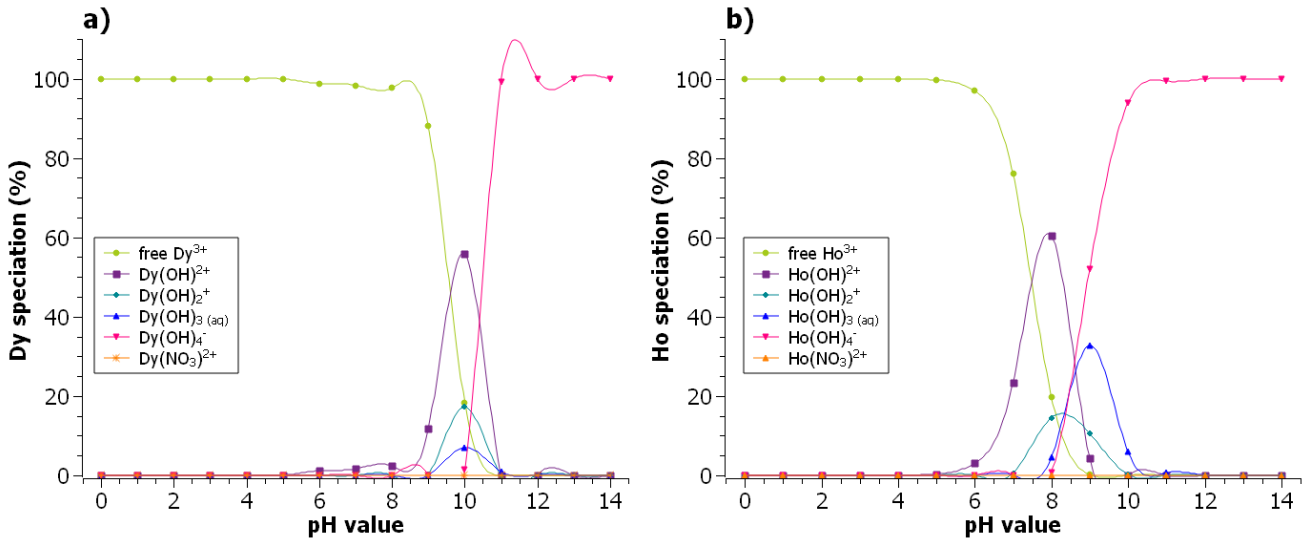

Figure 8. The speciation of a) Dy(III) ions in equilibrium with water as a function of pH (Dy(III) concentration = $0.084\ mM$, NO_3^- concentration = 0.252 mM). The speciation of b) Ho(III) ions in equilibrium with water as a function of pH (Ho(III) concentration = $1.18 \times 10^{-11} M$, NO_3^- concentration = 0.1 mM). These figures were data calculated by CHEAQS. For additional information, check Appendix B

Figure 9 shows the speciation for both Dy and Ho as a function of pH in an environment containing chlorides. In this case, the behaviour observed is very similar to that of the nitrates, as shown in Figure 8. In all cases, the dominant species are: free metal ions in acidic conditions, metal hydroxide cations at a pH of 8 in the case of Ho and 10 in the case of Dy, and metal hydroxide anions at basic conditions with a pH higher than 8 and 10. At experimental conditions, with a pH of 7.4, the dominant species is also already the metal hydroxide cation in the case of Ho and free Dy^{3+} ions in the case of Dy. Similar to before, from Figure 7, solid Dysprosium hydroxides were also expected, but the same issues with CHEAQS were found. From Figure 7 it is expected that Dy will speciate to around 5% positively charged $Dy(OH)^{2+}$ and around 75% solid $Dy(OH)_3$.

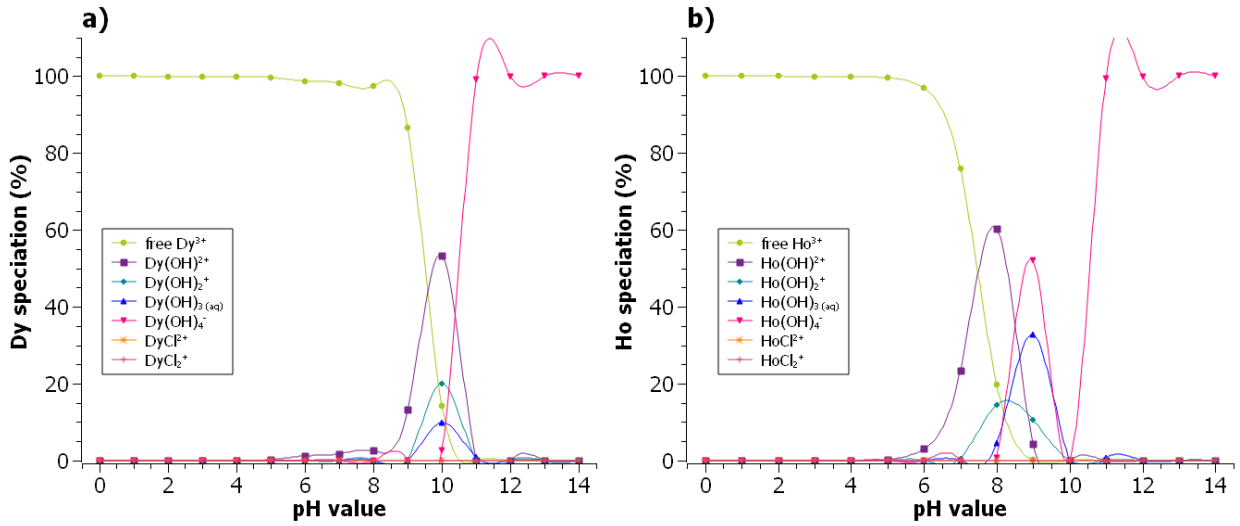

Figure 9. The speciation of a) Dy(III) ions in equilibrium with water as a function of pH (Dy(III) concentration = $0.074\ mM$, Cl^- concentration = 0.1 mM). The speciation of b) Ho(III) ions in equilibrium with water as a function of pH (Ho(III) concentration = $1.18 \times 10^{-11} M$, Cl^- concentration = 0.1 mM). These figures were data calculated by CHEAQS. For additional information, check Appendix B

Although the results were not optimal, loading was sufficiently high to allow for performing stability studies when using radioactive ^{166}Dy. Therefore, experiments were continued with ^{166}Dy.

4.3 Radiolabelling micelles with radioactive ^{166}Dy

The next tests were meant to function as a proof of concept to test radiolabelling efficiency and stability of the radiolabelling when using two different radioactive Dy sources. These two sources are: $Dy(NO_3)_3$ dissolved in water ('nitrate' source) when applying lower activity, and Dy_2O_3 dissolved in HCl ('oxide in HCl' source) when applying higher activity. The radiolabelling results can be seen in Figure 10 and Figure 11.

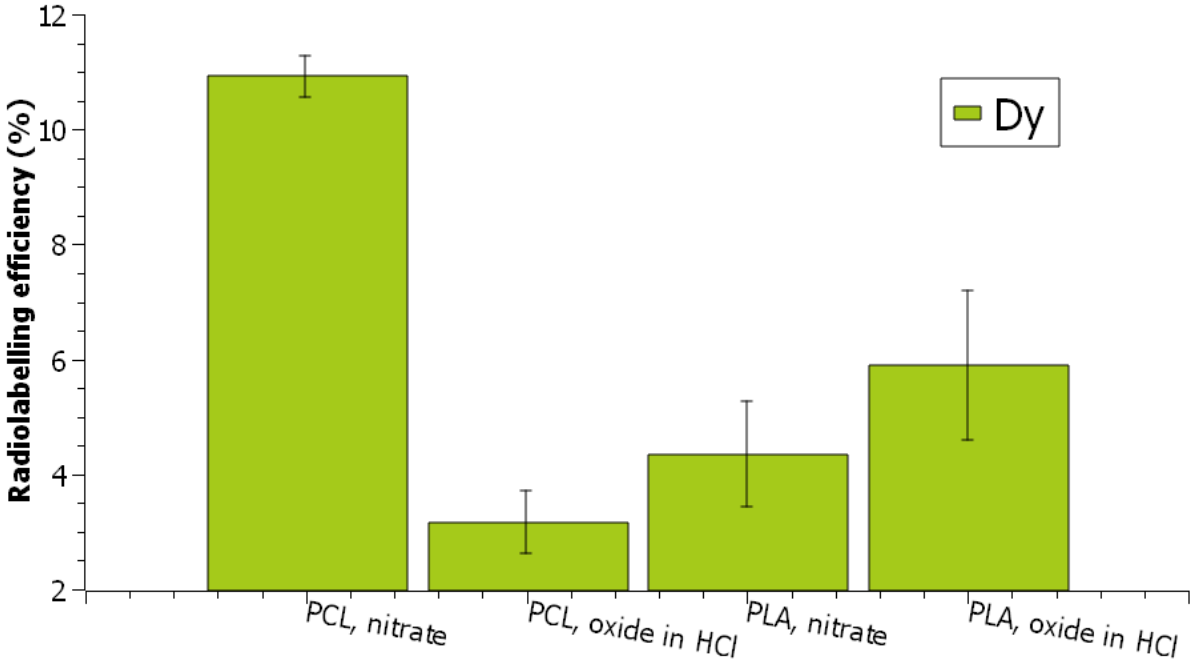

Figure 10. Radiolabelling efficiency achieved by the addition of irradiated Dy into PCL-PEO and PLA-PEO micelles from different radioactive sources. (Radioactivity per ml of micelle solution: 1 kBq/ml for nitrate sources and 10 kBq/ml or for oxide in HCl sources, total Dysprosium concentration: 0.084 mM for nitrate sources and 0.074 mM for oxide in HCl sources, polymer concentration: 4.3 mg/ml for PEO-PCL micelles and 2.5 mg/ml for PEO-PLA micelles in 10 mM HEPES buffer with pH of 7.4, radiolabelling time: 30 minutes under stirring, standard error based on 3 repeat experiments)

As seen in Figure 10, the radiolabelling efficiency of ^{166}Dy is the only one reported, even though, because of the way Dysprosium was irradiated, and cooled for 48 hours, ^{166}Ho is also present in the sample. The reason to only show ^{166}Dy is the difficulty to distinguish between ^{166}Dy and ^{166}Ho when using the NaI gamma activity counter (Wallac) Both ^{166}Dy and ^{166}Ho emit gammas at 81-82 keV, and the energy resolution of the Wallac does not allow separating the two peaks. However, ^{166}Dy also emits gammas at a window of 340-460 keV with a lower efficiency, so it is possible to discriminate the activity emitted by ^{166}Dy in this range. This means that only ^{166}Dy could be properly determined using this detector and this is why it was decided to only show the results for ^{166}Dy.

Figure 10 shows similar performance between PCL-PEO and PLA-PEO micelles, compared to what was shown in Figure 4. It is important to note that a direct comparison can only be made between the findings in Figure 4 and Figure 10 when it comes to the oxide in HCl source, since the anions present are more similar. In the case of PCL-PEO micelles, similar to the 2.81 ± 0.38 % loading efficiency achieved, a radiolabelling efficiency of 3.16 ± 0.55 % was achieved. Since the Dy concentrations used are very close (0.1 mM and 0.084 mM respectively) this was expected. What was unexpected, however, was the increase in radiolabelling efficiency when comparing the two Dy sources, where the radiolabelling efficiency using Dy-nitrate was significantly higher than using Dy-oxide (10.92 ± 0.35% and 3.16 ± 0.55 % respectively). From the speciation analysis, Dy-oxide micelles are very closely resembling the amount of $Dy(OH)^{2+}$ expected within the micelle solution (around 4%), while the increase in radiolabelling efficiency using the nitrate source probably shows the presence of Dysprosium hydroxide solids, which are the most dominant species in the experimental conditions. If this is true, it would be expected that the micelles loaded using the Dy-nitrate source may have higher stability when challenged with chelators such as DTPA.

In the case of the PLA-PEO micelles, results in both cases were not significantly different to the non-radioactive study, or to each other, and radiolabelling efficiencies also closely resembled the amount of $Dy(OH)^{2+}$ shown in Figure 7 (radiolabelling efficiency achieved was 4,35 ± 0.91% and 5,90 ± 1.30% respectively while the speciation shows that around 5% of the Dy speciates to $Dy(OH)^{2+}$). This probably means that the main species expected to be inside the micelle core is the $Dy(OH)^{2+}$ ion, and stability is not expected to be very high good. In both cases, the results are supporting the idea that metal hydroxides are expected to play an important role in the loading mechanism. This result matches what was already found by Liu [7], [8] for ^{111}In and ^{177}Lu. When looking at the speciation for both ^{111}In and ^{177}Lu , in both cases, the dominant species are metal hydroxides, with In speciating to $In(OH)_{3\,(aq)}$ at a percentage higher than 99%, and Lu speciating to $Lu(OH)^{2+}$, $Lu(OH)_2^{+}$ and $Lu(OH)_3$, all at 20-30% each. In this study radiolabelling efficiencies achieved were 83% and 91% respectively. Therefore, as long as aqueous metal hydroxides are present, radiolabelling seems to be able to occur.

Figure 11 shows that low stabilities were obtained for all samples when challenged with DTPA, i.e. the maximum retention in the micelles was 31±6.9%. In general, the stabilities achieved for both Dy and Ho ions in the presence of Cl^- were lower than what was achieved when using Dy-nitrate, but there was no a significant difference in the case of PCL-PEO micelles, which was unexpected due to the predictions made based on radiolabelling efficiency. Comparisons were made based on the DTPA fraction, due to the smaller error obtained in the Dy-nitrate experiments. As very low activities were used, experiments performed with the nitrate source presented a challenge when performing DTPA stability analysis, as the activity levels were close to gamma counter detection limit, and some measurements had to be repeated due to this. Stability was also affected by the speciation of both metals. It is expected that when metal hydroxide concentrations within the micelles are high enough, precipitation will occur spontaneously, thus keeping the metals inside the micelles. However, if the concentration inside the micelles does not reach the point at which precipitation occurs, metal hydroxide ions will be free to diffuse out of the micelles, thus reducing retention inside the micelles.

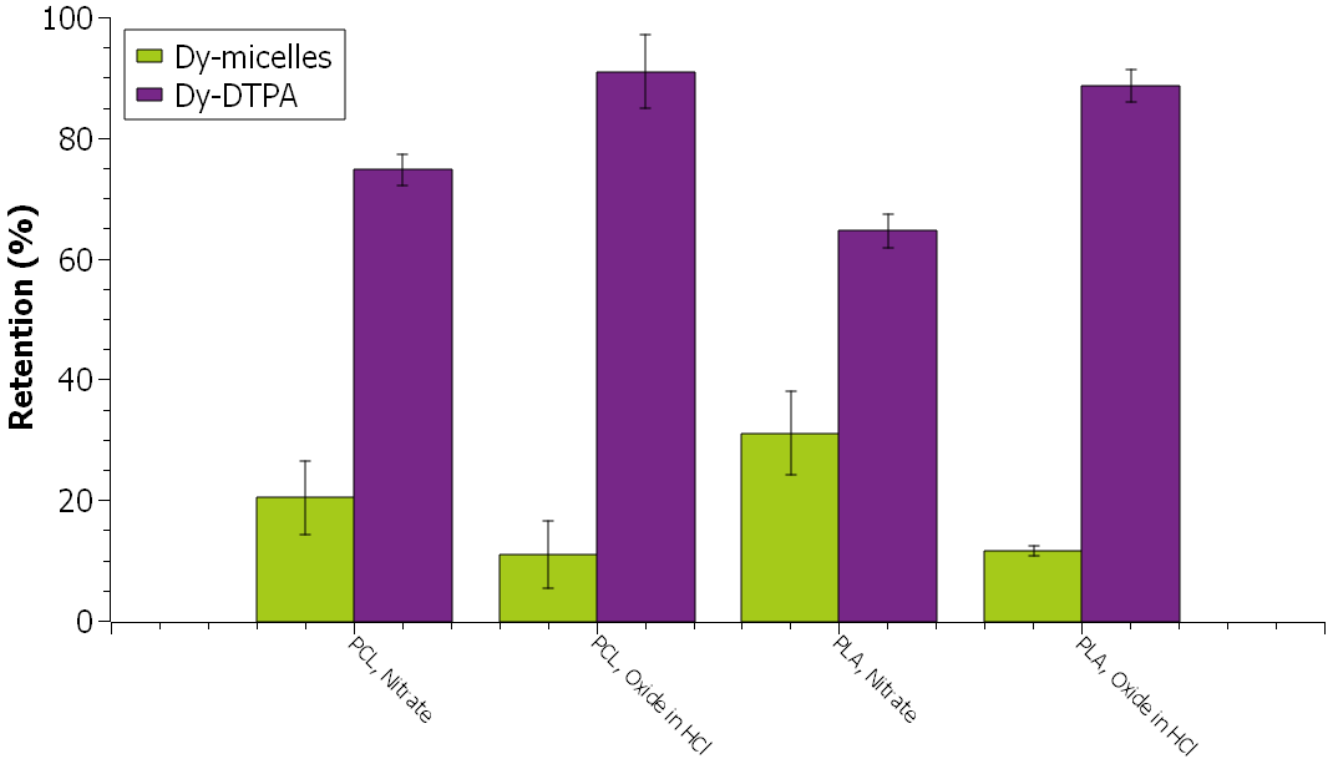

Figure 11. Stability analysis made on ^{166}Dy achieved by the addition of irradiated Dy (^{166}Dy) into PCL-PEO and PLA-PEO micelles from different activity sources. (Average activity added per ml of micelle solutions for radiolabelling: 1kBq/ml or 0.708 pM for nitrate source, and 10 kBq/ml or 7.08 pM for oxide in HCl source, DTPA concentration: 1mM in 10 mM HEPES buffer with pH of 7.4, polymer concentration: ~0.79 mg/ml for PEO-PCL micelles and ~0.45; mg/ml for PEO-PLA micelles, radiolabelling time: 30 minutes under stirring, standard error based on 3 repeat experiments)

The different speciation analysis performed helped explain both loading and radiolabelling efficiencies as shown in section 4.1. However, it was clear from the low efficiencies and stabilities achieved that only adding Dy either in the nitrate or oxide in HCl form is not sufficient to consider micelles as effective carriers for the *in vivo* generator. Therefore, alternative methods to induce the precipitation of Dy and Ho had to be considered to give micelles another chance. Liu et al. used three methods to attempt to induce the formation of Lu precipitates: increasing the pH of the solution, increasing metal concentration by adding non-active Lu to the radioactive ^{177}Lu solution or adding phosphate ions at different concentrations. The first method was not successful, and although the latter two methods were both successful in significantly increasing the stability of ^{177}Lu radiolabelling, the addition of phosphate ions was the more promising method. It achieved the retention of more than 90% of ^{177}Lu inside the micelles. Therefore, an evaluation on the use of phosphate ions to aid in inducing precipitation was carried out, starting with a speciation analysis.

4.4 Addition of phosphates

4.4.1 Speciation analysis on Dy nitrates and chlorides

Figure 12 shows the speciation of Dy ions in equilibrium as a function of the addition of phosphate ions, when using Dy-nitrate salts. Phosphate ions were selected because it is known that they interact with lanthanide ions to form insoluble salts [48]. Although other ions were attempted such as carbonates, sulphates and even sulphides, no other anions appeared to result in Dy precipitates. Because the concentration of Ho ions is so much lower than the concentration of Dy ions present in the micelle solution, and because the measurements performed and reported are for Dy ions, and not Dy and Ho ions, only the speciation for Dy was considered significant.

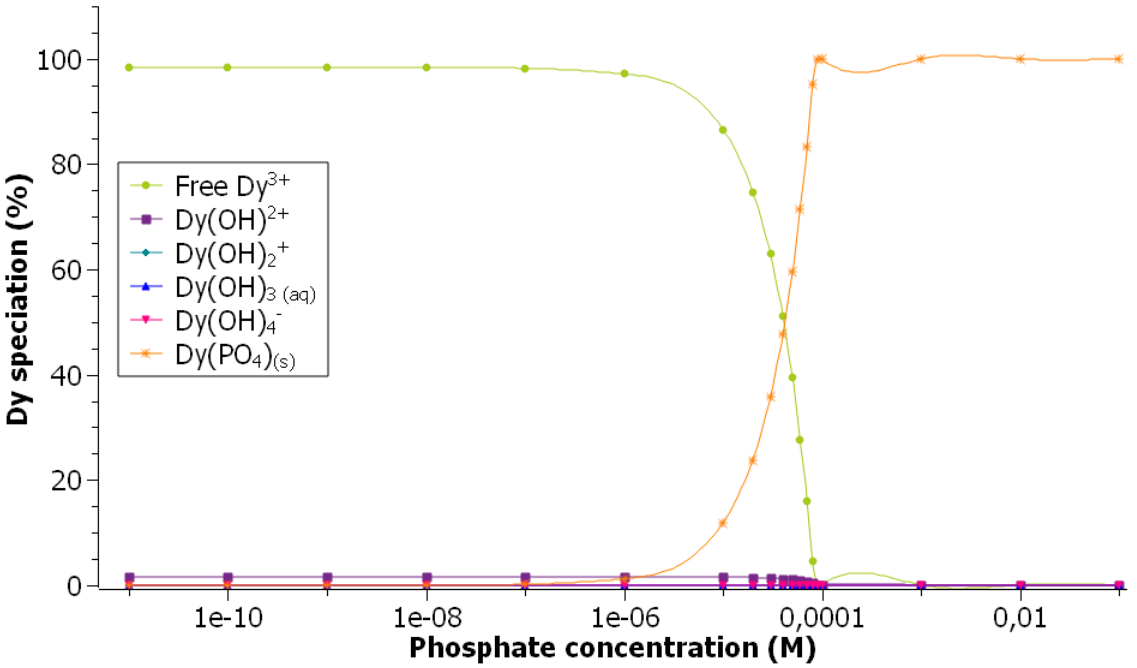

Figure 12. The speciation of Dy(III) ions in equilibrium with water as a function of phosphate concentration (Dy(III) concentration = 0.084 mM, NO3- concentration = 0.252 mM, pH = 7). These figures were data calculated by CHEAQS. For additional information, check Appendix B

Figure 13 shows the effect of Dy speciation as a function of phosphate concentration in a chloride environment. In the same way as before, a speciation for Ho was not performed, because of how much more significant the concentration of Dy was in the tests performed. As before, other anions were tested as candidates to aid in the precipitation of Dy, but none were as successful as phosphate ions. As mentioned in section 2.3.3, and similar to the analysis at section 4.4, it would be expected that the addition of phosphates will lead to an increase in radiolabelling stability, as Dy will readily precipitate to Dy phosphate. However, this is only true if precipitation happens inside the micelle core. This is because it is still unknown how readily $Dy(PO_3)$ will diffuse into the micelle core, but it is expected that, as was the case when the concentration of solid $Dy(OH)_3$ was too high, the radiolabelling will become erratic and thus less desirable for the process.

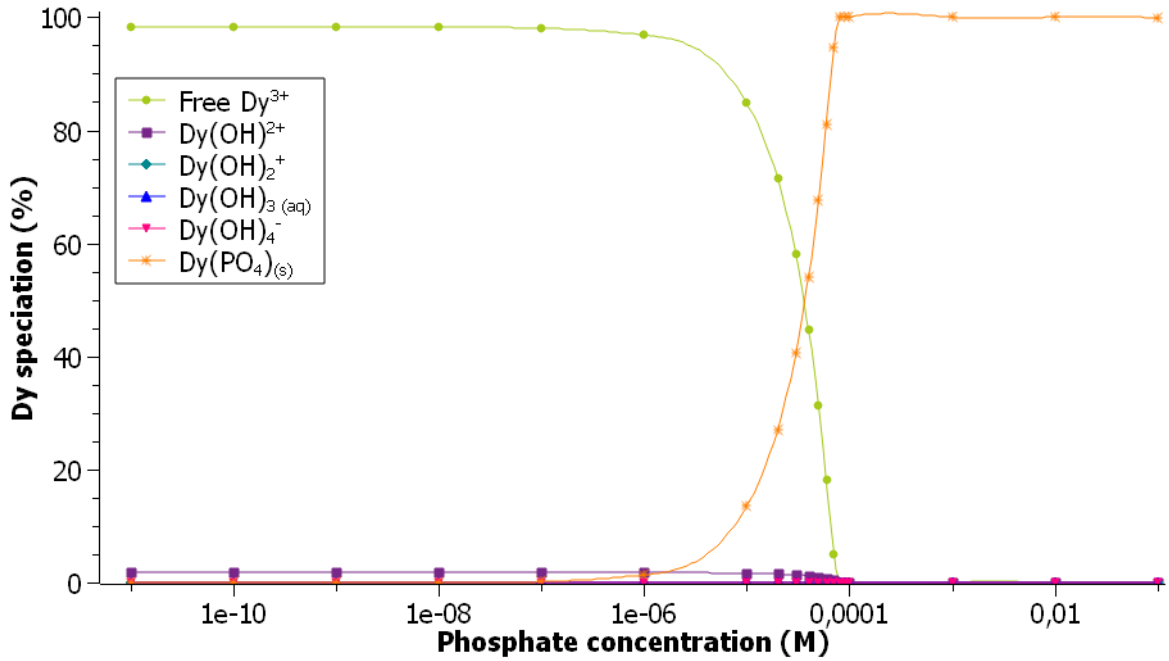

Figure 13. The speciation of Dy(III) ions in equilibrium with water as a function of phosphate concentration (Dy(III) concentration = 3.58× 10 $^{-11}$ M, Cl^- concentration = 0.1 mM, pH = 7). These figures were data calculated by CHEAQS. For additional information, check Appendix B.

As seen on Figure 12 and Figure 13, similar to an increase in metal concentration, the addition of phosphates leads to precipitation. However, the precipitates formed are solid metal phosphates, as opposed to the solid metal hydroxides formed before. In fact, the metal phosphates formed become dominant after the addition of between 10^{-4} and 10^{-5} M phosphate ions in the case of the nitrate source, and between 10^{-3} and 10^{-5} M in the case of the oxide in HCl source. Based on these results, experiments were designed as explained in sections 4.4.2 and 4.4.3 to evaluate the effect adding phosphates has on both loading and stability.

4.4.2 Radiolabelling micelles using irradiated $Dy(NO_3)_3$ dissolved in water

Because the metal concentration was not having a good enough effect on radiolabelling to ensure a good enough radiolabelling efficiency, the next set of experiments performed tried to use the addition of phosphates to improve on the radiolabelling efficiency. In the case of the Dy-nitrate source the concentration of phosphates tested experimentally were selected from the speciation shown in Figure 12. The selected concentrations were meant to induce phosphate ions, but were selected to be at the low side, to avoid inducing precipitation prior to the hydroxides entering the micelles. For comparison purposes, a lower concentration (10^{-7} M) and a higher concentration (10^{-6} M) of phosphates were selected. Figure 14 Shows the obtained results.

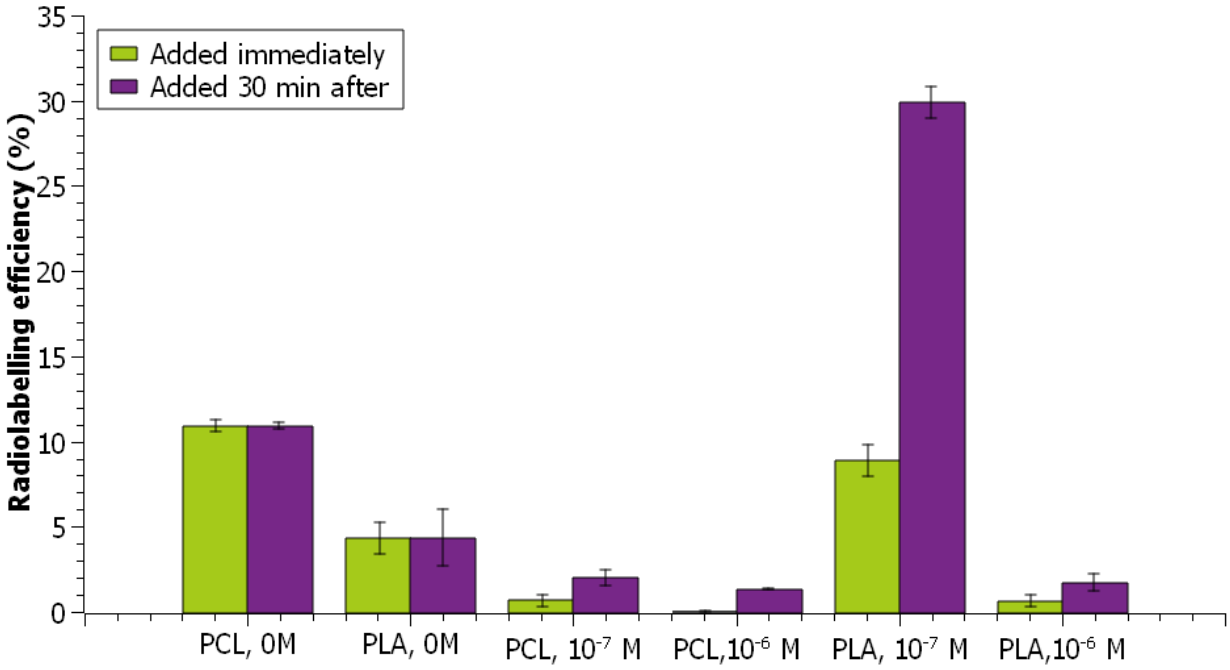

Figure 14. The radiolabelling efficiency achieved by adding two different concentrations of phosphate ions. The phosphate ions were added immediately before adding activity (in green) and 30 min after adding activity (in purple) on PCL-PEO and PLA-PEO micelles. (Activity per ml of micelle solution: 1 kBq/ml of micelle solution, Dy concentration: 0.084 mM, polymer concentration: 4.3 mg/ml for PEO-PCL micelles and 2.5 mg/ml for PEO-PLA micelles in 10 mM HEPES buffer with pH of 7.4, standard error based on 3 repeat experiments)

The addition of phosphates was expected to induce metal precipitation within the micelle core, based on the already accumulated Dysprosium hydroxide ions in the micelle core. This should ensure stable encapsulation of the metals inside the micelles, as solid aggregations would not as readily diffuse out of the micelles as aqueous metal hydroxides. As can be seen in Figure 14, it is possible to observe that the additions of phosphate ions at different time points had very different effect on the radiolabelling efficiency of both types of micelles.

Adding phosphates 30 minutes after ^{166}Dy addition led to an increase in radiolabelling efficiency in all cases. A likely explanation in this case could be that the addition of phosphates shifts the equilibrium of the system, leading to the precipitation of $Dy(PO_4)$. Therefore, when adding phosphates before the addition of Dysprosium, it is less likely that Dy hydroxides are formed, and, as stated before, they are the most important species for radiolabelling. Meanwhile, if Dy hydroxides have already been able to enter the micelle core, the expectation is that phosphates will diffuse into the micelle core, and, if the concentration is high enough, precipitation can be expected within the micelle core, which is desired. This is mostly supported by the behaviour of PCL-PEO micelles in general. However, this does not fully

explain how the addition of 10^{-7} M phosphates led to an increase in radiolabelling efficiency, even when added immediately before the activity was added.

It is important to note that the concentration within a specific micelle is unknown in this work, and that all predictions performed are done based on the total concentrations in solution. Therefore, it is possible that the lower concentration of metals that diffuse into the core require a lower phosphate concentration to induce precipitation, explaining the increase in radiolabelling efficiency when adding a low phosphate concentration immediately before adding activity. This would also mean that stability should be higher in this case. However, because of the low activities used when performing Dy-nitrate experiments, stability measurements were not possible in most cases.

When adding phosphates at a concentration of 10^{-7}M the behaviour of the different types of micelles differed more significantly than in cases where no phosphates were added. When adding this phosphate concentration to PCL-PEO micelles a decrease in radiolabelling efficiency was observed instead. Meanwhile, when adding phosphates at this concentration to PLA-PEO micelles a significant increase in loading was seen. A possible theory that might explain this different behaviour is that the size of the PCL-PEO and PLA-PEO micelles differed, with the PLA-PEO micelles being much larger. However, if micelle size was the issue, saturation would be expected. Here, the addition of phosphates would not lead to a significant increase or decrease in radiolabelling efficiency. Instead, Figure 14 shows a decrease in radiolabelling efficiency. Therefore, the observed change might be due to the difference in water volume found in the micelle core.

As mentioned in section 2.3.2, the carbonyl groups present in the hydrophobic part of PCL-PEO and PLA-PEO micelles provides the ability to make hydrogen bonds with water, and makes the core slightly more hydrophilic than that of other micelles, such as Polystyrene-block-Polyethylene oxide and Polybutadiene-block-Polyethylene oxide. This explained why these micelles had higher radiolabelling efficiencies as reported by Liu et al. [8]. However, it is possible that PLA is more capable of forming hydrogen bonds than PCL, making its core more hydrated. The findings of Dahal et al. show that, although hydrogen bonds in PCL-PEO micelles are formed, they tend to be closer to the core-corona interface, as evidenced by the lower than expected water permeation in the micelle core [39]. This implies that these micelle cores may be more hydrophobic than expected and explain the lower radiolabelling efficiency achieved. Meanwhile, the findings of Leson et al. showed the capability of PLA-PEO vesicles to form hydrogen bonds, possibly resulting in the temporary localization of water molecules across the vesicle membrane [46]. As the mechanism behind loading micelles used in this report is diffusion based, the water permeability of the micelles may have a more important role in achieving successful radiolabelling, and explains why PLA-PEO micelles have consistently resulted in higher radiolabelling efficiencies than PCL-PEO micelles.

4.4.3 Radiolabelling micelles using irradiated [^{166}Dy]Dy_2O_3 dissolved in HCl

To continue the investigation on the effect of adding phosphate ions into the micelle solution on the radiolabelling efficiency, loading and stability tests were performed on micelles radiolabelled with higher activities, achieved by irradiating Dy_2O_3 instead of $Dy(NO_3)_3$, and subsequently dissolving the Dy_2O_3 in HCl. To select the phosphate concentrations to use in this set of experiments, the speciation in Figure 13 was used. Here, similarly to the speciation when using nitrates, phosphate ions readily precipitate Dy into $Dy(PO_4)$. However, this occurs at slightly lower concentrations than in the case of Figure 12. This led to a different selection of phosphate concentrations to add when performing labelling experiments with the addition of phosphates. Based on the same logic as explained in section 4.4.2, a low ($3 \times 10^{-8}\ M$) and a high concentration (10^{-7} M) were selected. The radiolabelling efficiency achieved can be seen in Figure 15 and the radiolabelling stability results are shown in Figure 16

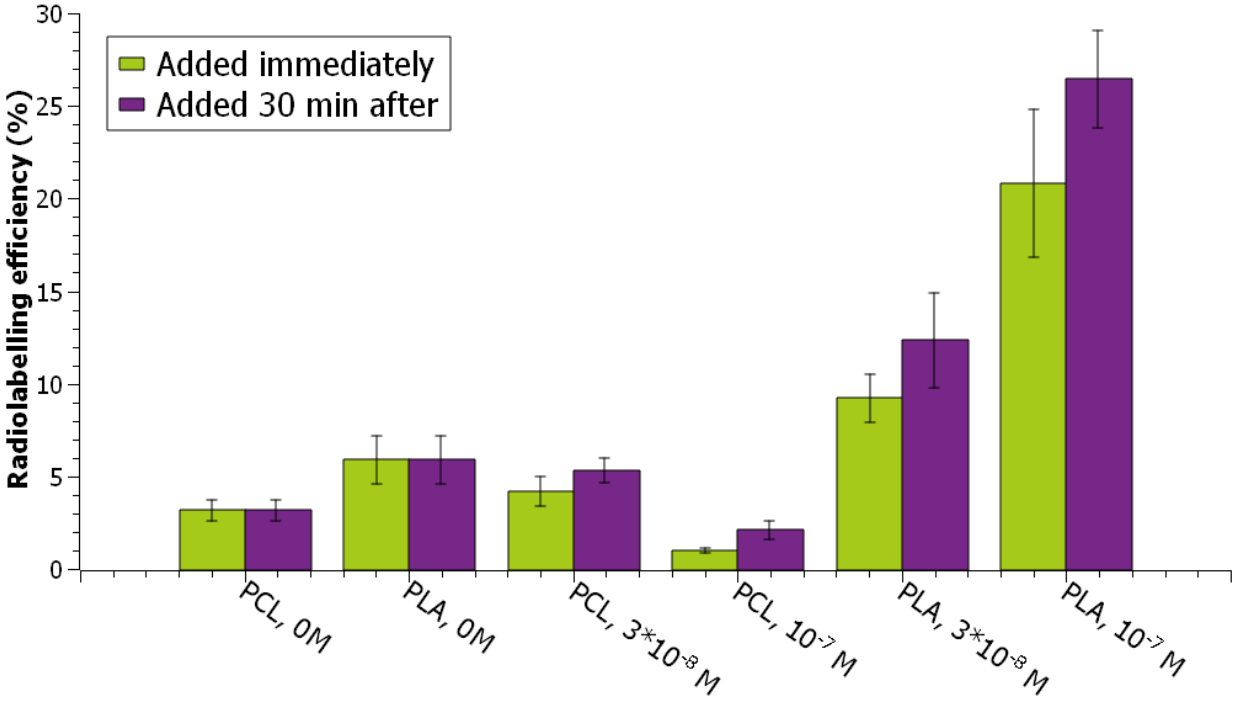

Figure 15. Radiolabelling efficiency achieved by adding two different amounts of phosphate ions immediately before adding activity (in green) and 30 min after adding activity (in purple) on PCL-PEO and PLA-PEO micelles. (Activity per ml of micelle solution: 10 kBq/ml, Dy concentration: 0.074 mM, polymer concentration: 4.3 mg/ml for PEO-PCL micelles and 2.5 mg/ml for PEO-PLA micelles in 10 mM HEPES buffer with pH of 7.4, standard error based on 3 repeat experiments)

Figure 15 shows the radiolabelling efficiency achieved when adding different phosphate concentrations to the micelle solution. This time, phosphate concentrations added to the micelle solution were lower, because, as shown in Figure 13, solid Dysprosium Phosphate dominates the speciation at lower concentrations. As mentioned before, it was not desired to induce the precipitation of phosphate ions too early in the process. In this case, both polymer micelles reached higher radiolabelling efficiency as a result of the addition of phosphates during different experiments. For PCL-PEO micelles, the lower phosphate concentration did lead to an increase in radiolabelling efficiency, even if the final efficiencies are still quite low. However, the higher phosphate concentration led to a lower radiolabelling efficiency, regardless of when the phosphates were added, similarly to the results found in Figure 14. Meanwhile, for PLA-PEO micelles, the addition of phosphates consistently led to higher radiolabelling efficiencies, with smaller increases caused by the addition of less phosphates and larger increases caused by the addition of more phosphates. For both micelles, there was consistently an increase in the radiolabelling efficiency when adding phosphates after 30 minutes rather than immediately.

In these experiments, the behaviour of PLA-PEO micelles was as expected, where the addition of phosphates was always correlated with an increase in radiolabelling efficiency. This implies that in this case, the shift in equilibrium towards the precipitation of metal phosphates within the micelles is very beneficial for the radiolabelling efficiency. The effect of adding phosphate ions after allowing 30 min for entering of possible hydroxides into the core shows that the addition of phosphates leads to a reduction in the ability of Dy to diffuse out of the micelle core, leading to a higher radiolabelling efficiency. Another interesting result from this experiment is that when adding a phosphate concentration of 10^{-7}M into a PLA-PEO micelle solution 30 minutes after adding the radioactive metal solution led to similar radiolabelling efficiencies, regardless of what Dy source was used. When working with a lower activity in the nitrate source, a Dy radiolabelling efficiency of 29.90 ± 0.22% was achieved, while when performing the same experiment with a higher activity in the oxides in HCl source led to a total radiolabelling efficiency of 26.45 ± 2.63%. This result shows that the addition of phosphates helps making the process independent of the irradiated Dy compound, which is very desirable for future applications, and further shows that the main purpose for adding phosphate ions into the solution is to induce precipitation and avoid the ability of aqueous metal hydroxides to diffuse out of the membrane core.

Meanwhile, the behaviour of PCL-PEO micelles was still unexpected. At lower phosphate concentration, the observed behaviour is as expected, but upon adding a larger phosphate concentration lower loading efficiency is observed compared to not adding phosphates at all. This might also be explained by the lower permeability of PCL-PEO micelles compared to PLA-PEO micelles, as well as the lower radiolabelling efficiencies in the first place. As the radiolabelling efficiency is very low, most of the Dy is still in the micelle solution, so the addition of phosphates might lead to premature precipitation of Dy in the micelle solution. As the concentration of Dy is higher than that of phosphates in the micelle solution, it is likely that this would lead to less diffusion of phosphate ions to the micelle core. This would leave metal hydroxides inside the micelle core to freely diffuse out of it.

Figure 16 shows the results of the DTPA stability challenge performed on micelles that were radiolabelled in the same way as in Figure 15. Here, it is possible to observe that the addition of phosphates did not, for the most part, lead to an increase in radiolabelling stability, with certain exceptions. In most cases, around 10% of the activity measured remained in the micelles, while around 90% was found either as a complex with DTPA or as free ions. The DTPA stability test is made to quantify the proportion of metal ions that can be removed from the micelles , that is, the ones that are free to be complexed with DTPA. From the method explained in section 2.3.3, the metal that is encapsulated into the micelles and remains in them is the one that has been able to precipitate within the micelles. If a low stability is achieved, this means that a low percentage of Dy reached the concentration that was needed for the precipitation to occur. Unfortunately, it would be very complicated to control the concentration of metals within each micelle in a way that is predictable and repeatable, so all changes that can be made bust be done on a larger scale, i.e. in the micelle solution and not in each micelle. The two parameters that are likely to make a difference in this case are phosphate concentration, which could be increased to a point where precipitation more readily occurs and increasing the time after phosphate ions were added to allow for more precipitation.

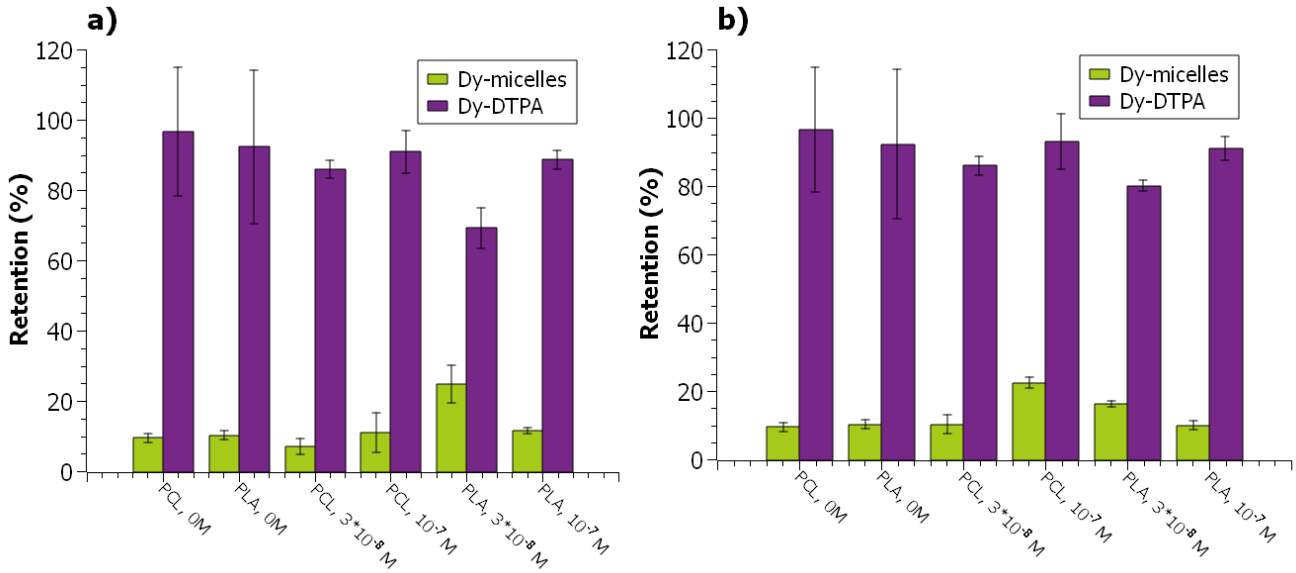

Figure 16.The retention of Dy in micelles when challenged with DTPA for the PCL-PEO and PLA-PEO micelles after loading them, with the addition of phosphates happening a) immediately before adding activity and b) 30 min after adding activity (purple). (Average activity added per ml of micelle solutions for radiolabelling: 10 kBq/ml solution or 7.08 pM, DTPA concentration: 1mM in 10 mM HEPES buffer with pH of 7.4, polymer concentration: ~0.79 mg/ml for PEO-PCL micelles and ~0.45; mg/ml for PEO-PLA micelles, standard error based on 3 repeat experiments)

From the results obtained, both of these parameters could have an effect on radiolabelling efficiency and stability. In the case of increasing phosphate ion concentration, as long as 30 minutes are allowed to avoid premature precipitation, an increase in phosphate concentration might be beneficial to radiolabelling efficiency and stability. This allows Dy hydroxide ions to be within the micelle core before inducing precipitation, and avoids the stochastic nature

of solid transport into the micelle core. Although a premature precipitation was attempted to avoid in this work, it is expected that phosphate ion concentrations lower than 0.1 mM can increase the radiolabelling stability.

The radiolabelling time could have such an effect, because there is no clear pattern as to what phosphate concentrations led to significantly better stabilities. However, the only stabilities that showed to be significantly better than the rest are the addition of 10^{-7} M phosphates in the PCL-PEO micelles, 30 minutes after the addition of the radioactive metal and the addition of $3 \times 10^{-8} M$ phosphates to the PLA-PEO micelles, 30 minutes after the addition of the active metal. The Dy radiolabelling efficiencies in the most stable micelles were of 2.11 ± 0.50 % in the PCL-PEO micelles and 12.35 ± 2.57% in the PLA-PEO micelles. Neither of these was the highest loading achieved for the micelles, and yet they were the most stable. The only thing they have in common is the fact that phosphates were added 30 min after the addition of the radioactive Dy. Although the other cases where the addition of phosphates occurred 30 min after the addition of the radioactive metal solution did not lead to a significantly better stability, this development shows that inducing precipitation using phosphates has led to an increase in stability. It is possible that the stability could be further increased through allowing a longer time for phosphates to induce precipitation in the micelle cores, that is, by stirring for longer than 30 minutes after the addition of phosphates. It is possible that the plateau has not been reached after 30 minutes, which would explain that not all phosphate additions led to significantly better stabilities, as the diffusion coefficient of phosphate ions entering the micelle core in unknown.

However, much needs to be understood to really tune the radiolabelling of the micelles ensuring good radiolabelling efficiency and stability, and the best way to achieve this is to further understand the best way to induce precipitation via the addition of phosphates.

5 Conclusions and Recommendations

As can be seen from the results achieved in this report, first steps have been made to make micelles promising nanocarriers for a system containing ^{166}Dy. However, many steps still need to be researched to find out whether micelles can function as effective nanocarriers for a ^{166}Dy/^{166}Ho *in vivo* generator.

The current work was able to show that the radiolabelling mechanism is reliant upon the diffusion of aqueous metal hydroxides to enter the micelle core, and then something that induces the precipitation of the metal, in this case Dysprosium, inside the micelle core, not allowing it to diffuse out, thus increasing radiolabelling efficiency and stability. This was especially evidenced by how the radiolabelling efficiencies in experiments without the addition of phosphates resembled the percentage of Dy that speciated into $Dy(OH)^{2+}$.

Although the results obtained were not as good as what was found by Liu et al. in the radiolabelling with ^{111}In and ^{177}Lu, it is possible to say that, overall, the most promising radiolabelled micelles found in this study are PLA-PEO micelles, which were radiolabelled and then phosphate ions were added at a concentration of $3 \times 10^{-8} M$, 30 minutes after the addition of the radioactive metal. Although PLA-PEO micelles where a higher phosphate concentration was added led to a higher radiolabelling efficiency, their stability was not as good.

The next step in this process would be to understand the kinetics behind radiolabelling micelles after the addition of phosphates, to be able to tune the radiolabelling process and increase both radiolabelling efficiency and stability. This can be done by allowing Dysprosium hydroxides to diffuse into the micelle core, followed by inducing precipitation through the use of phosphates. It has been shown that the addition of phosphates can improve both, so finding the best conditions for this to be accomplished is essential.

Another recommendation to continue this study is that, after further understanding the effect that the addition of phosphates has on the kinetics behind radiolabelling the micelles, further stability tests must be performed. The next step should be based on the performance of the radiolabelled micelles in presence of serums that assimilate the system to physiological conditions. Eventually, *in vitro* and *in vivo* tests must be performed to observe the behaviour of radiolabelled micelles in conditions that have further similarities to the conditions at which RNT is applied to patients.

References

[1] 'Cancer', WHO, Fact sheet, Feb. 2022. Accessed: May 22, 2022. [Online]. Available: https://www.who.int/news-room/fact-sheets/detail/cancer

[2] A. Dash, F. F. Knapp, and M. Pillai, 'Targeted Radionuclide Therapy - An Overview', *Curr. Radiopharm.*, vol. 6, no. 3, pp. 152–180, Oct. 2013, doi: 10.2174/18744710113066660023.

[3] N. J. M. Klaassen, M. J. Arntz, A. Gil Arranja, J. Roosen, and J. F. W. Nijsen, 'The various therapeutic applications of the medical isotope holmium-166: a narrative review', *EJNMMI Radiopharm. Chem.*, vol. 4, no. 1, p. 19, Dec. 2019, doi: 10.1186/s41181-019-0066-3.

[4] 'Live Chart of Nuclides: nuclear structure and decay data', IAEA. Accessed: May 22, 2022. [Online]. Available: https://www-nds.iaea.org/relnsd/vcharthtml/VChartHTML.html

[5] S. V. Smith, N. Di Bartolo, S. Mirzadeh, R. M. Lambrecht, F. F. Knapp, and E. L. Hetherington, '[166Dy]Dysporium/[166Ho]Holmium In Vivo generator', *Appl. Radiat. Isot.*, vol. 46, no. 8, pp. 759–764, Aug. 1995, doi: 10.1016/0969-8043(94)00149-T.

[6] P. E. Edem, J. Fonslet, A. Kjær, M. Herth, and G. Severin, 'In Vivo Radionuclide Generators for Diagnostics and Therapy', *Bioinorg. Chem. Appl.*, vol. 2016, p. 6148357, 2016, doi: 10.1155/2016/6148357.

[7] H. Liu, 'Application of poly(ε-caprolactone-b-ethylene oxide) micelles combined with ionizing radiation in cancer treatment', TU Delft, Delft, The Netherlands, 2021.

[8] H. Liu *et al.*, 'Efficient radiolabeling of block copolymer micelles through radiometal salt precipitation for theranostic applications'.

[9] D. Ersahin, I. Doddamane, and D. Cheng, 'Targeted Radionuclide Therapy', *Cancers*, vol. 3, no. 4, pp. 3838–3855, Oct. 2011, doi: 10.3390/cancers3043838.

[10] S. Srivastava and E. Dadachova, 'Recent Advances in Radionuclide Therapy', p. 12.

[11] C. A. Hoefnagel, 'Radionuclide cancer therapy', *Ann. Nucl. Med.*, vol. 12, no. 2, pp. 61–70, Apr. 1998, doi: 10.1007/BF03164831.

[12] C. Beijst, B. Kunnen, M. G. E. H. Lam, and H. W. A. M. de Jong, 'Technical Advances in Image Guidance of Radionuclide Therapy', *J. Nucl. Med. Technol.*, vol. 45, no. 4, pp. 272–279, Dec. 2017, doi: 10.2967/jnmt.117.190991.

[13] U. Hennrich and K. Kopka, 'Lutathera®: The First FDA- and EMA-Approved Radiopharmaceutical for Peptide Receptor Radionuclide Therapy', *Pharmaceuticals*, vol. 12, no. 3, p. 114, Jul. 2019, doi: 10.3390/ph12030114.

[14] 'Novartis reports clinically relevant improvement in median overall survival data in final analysis of pivotal NETTER-1 study with targeted radioligand therapy Lutathera', Novartis, Basel, Jun. 2021. [Online]. Available: https://www.novartis.com/news/media-releases/novartis-reports-clinically-relevant-improvement-median-overall-survival-data-final-analysis-pivotal-netter-1-study-targeted-radioligand-therapy-lutathera

[15] J. Ma, L. Li, T. Liao, W. Gong, and C. Zhang, 'Efficacy and Safety of 225Ac-PSMA-617-Targeted Alpha Therapy in Metastatic Castration-Resistant Prostate Cancer: A Systematic Review and Meta-Analysis', *Front. Oncol.*, vol. 12, p. 796657, Feb. 2022, doi: 10.3389/fonc.2022.796657.

[16] Endocyte, 'AcTION: A Phase I Study of 225Ac-PSMA-617 in Men With PSMA-positive Prostate Cancer and Extensive Skeletal Metastases', clinicaltrials.gov, Clinical trial registration NCT04597411, Feb. 2022. Accessed: Jun. 15, 2022. [Online]. Available: https://clinicaltrials.gov/ct2/show/NCT04597411

[17] A. I. Kassis and S. J. Adelstein, 'Radiobiologic Principles in Radionuclide Therapy', p. 9.

[18] L. J. Scott and J. C. Yanch, 'Absorbed dose profiles for radionuclides of frequent use in radiation synovectomy', *Arthritis Rheum.*, vol. 34, no. 12, pp. 1521–1530, 1991, doi: 10.1002/art.1780341208.

[19] S. Giralt *et al.*, '166Ho-DOTMP plus melphalan followed by peripheral blood stem cell transplantation in patients with multiple myeloma: results of two phase 1/2 trials', *Blood*, vol. 102, no. 7, pp. 2684–2691, Oct. 2003, doi: 10.1182/blood-2002-10-3250.

[20] N. T. Ueno *et al.*, 'Pilot Study of Targeted Skeletal Radiation Therapy for Bone-Only Metastatic Breast Cancer', *Clin. Breast Cancer*, vol. 9, no. 3, pp. 173–177, Aug. 2009, doi: 10.3816/CBC.2009.n.028.

[21] T. Das *et al.*, 'Preparation and animal biodistribution of166Ho labeled DOTA for possible use in intravascular radiation therapy (IVRT)', *J. Label. Compd. Radiopharm.*, vol. 46, no. 3, pp. 197–209, Mar. 2003, doi: 10.1002/jlcr.657.

[22] Y.-D. Hong, S.-J. Choi, S.-M. Choi, and B.-S. Jang, 'The availability of contrast media in the application of Holmium-166-DTPA for vascular brachytherapy', *Nucl. Med. Biol.*, vol. 31, no. 2, pp. 225–230, Feb. 2004, doi: 10.1016/j.nucmedbio.2003.08.006.
[23] J. Kim, Z.-X. Luo, Y. Wu, X. Lu, and M. Jay, 'In-Situ Formation of Holmium Oxide in Pores of Mesoporous Carbon Nanoparticles as Substrates for Neutron-Activatable Radiotherapeutics', *Carbon*, vol. 117, pp. 92–99, Jun. 2017, doi: 10.1016/j.carbon.2017.02.085.
[24] M. Lam, 'Adjuvant Hepatic Holmium-166-radioembolization in Patients With Unresectable Liver Metastases of Neuroendocrine Origin, Who Have Been Treated With Lutetium-177-dotatate', clinicaltrials.gov, Clinical trial registration NCT02067988, Jun. 2020. Accessed: Jun. 15, 2022. [Online]. Available: https://clinicaltrials.gov/ct2/show/NCT02067988
[25] M. Lam, 'Holmium-166-radioembolization in Patients With Unresectable Hepatocellular Carcinoma (HCC); a Multi-center, Interventional, Non-randomized, Non-comparative, Open Label, Early Phase II Study: HEPAR Primary', clinicaltrials.gov, Clinical trial registration NCT03379844, Dec. 2017. Accessed: Jun. 15, 2022. [Online]. Available: https://clinicaltrials.gov/ct2/show/NCT03379844
[26] MCBurgmans, 'HOlmium Radioembolization as Adjuvant Treatment to Radiofrequency Ablation for Early STage Hepatocellular Carcinoma (HORA EST HCC)', clinicaltrials.gov, Clinical trial registration NCT03437382, Mar. 2021. Accessed: Jun. 15, 2022. [Online]. Available: https://clinicaltrials.gov/ct2/show/NCT03437382
[27] B. A. Zonnenberg, 'Radioactive Holmium Microspheres for the Treatment of Patients With Unresectable Liver Metastases; a Single Center, Interventional, Non-randomized, Phase II (HEPAR II) Trial', clinicaltrials.gov, Clinical trial registration study/NCT01612325, Aug. 2015. Accessed: Jun. 15, 2022. [Online]. Available: https://clinicaltrials.gov/ct2/show/study/NCT01612325
[28] M. L. Smits *et al.*, 'Holmium-166 radioembolization for the treatment of patients with liver metastases: design of the phase I HEPAR trial', *J. Exp. Clin. Cancer Res. CR*, vol. 29, no. 1, p. 70, Jun. 2010, doi: 10.1186/1756-9966-29-70.
[29] K. Memon, R. J. Lewandowski, L. Kulik, A. Riaz, M. F. Mulcahy, and R. Salem, 'Radioembolization for primary and metastatic liver cancer', *Semin. Radiat. Oncol.*, vol. 21, no. 4, pp. 294–302, Oct. 2011, doi: 10.1016/j.semradonc.2011.05.004.
[30] J.-V. Kratz and K. H. Lieser, 'Radioactive decay kinetics', in *Nuclear and radiochemistry. Fundamentals and Applications*, 3rd ed., vol. 1, 2 vols, Weinheim, Germany: Wiley, 2013, pp. 189–205.
[31] G. Ferro-Flores *et al.*, '[166Dy]Dy/166Ho hydroxide macroaggregates: an in vivo generator system for radiation synovectomy', *Appl. Radiat. Isot.*, vol. 61, no. 6, pp. 1227–1233, Dec. 2004, doi: 10.1016/j.apradiso.2004.04.018.
[32] G. Ferro-Flores *et al.*, 'Labeling of biotin with [166Dy]Dy/166Ho as a stable in vivo generator system', *Int. J. Pharm.*, vol. 255, no. 1–2, pp. 129–138, Apr. 2003, doi: 10.1016/S0378-5173(03)00052-8.
[33] M. Pedraza-López, G. Ferro-Flores, C. A. de Murphy, J. I. Tendilla, and O. Villanueva-Sánchez, 'Preparation of (166)Dy/(166)Ho-EDTMP: a potential in vivo generator system for bone marrow ablation', *Nucl. Med. Commun.*, vol. 25, no. 6, pp. 615–621, Jun. 2004, doi: 10.1097/01.mnm.0000126516.57329.07.
[34] '22.10: Chelating Agents', *Chemistry LibreTexts*, May 09, 2016. https://chem.libretexts.org/Bookshelves/General_Chemistry/Book%3A_ChemPRIME_(Moore_et_al.)/22%3A_Metals/22.10%3A_Chelating_Agents (accessed May 26, 2022).
[35] A. J. Amoroso, I. A. Fallis, and S. J. A. Pope, 'Chelating agents for radiolanthanides: Applications to imaging and therapy', *Coord. Chem. Rev.*, vol. 340, pp. 198–219, Jun. 2017, doi: 10.1016/j.ccr.2017.01.010.
[36] J. R. Zeevaart, Z. Szucs, S. Takacs, J. Rooyen, and D. Jansen, 'Recoil and conversion electron implications to be taken into account in the design of therapeutic radiopharmaceuticals utilising in vivo generators', *J. Label. Compd. Radiopharm.*, vol. 55, no. 3, pp. 115–119, Mar. 2012, doi: 10.1002/jlcr.2906.
[37] J. R. Zeevaart, Z. Szücs, S. Takács, N. V. Jarvis, and D. Jansen, 'Recoil and conversion electron considerations of the ^{166} Dy/ ^{166} Ho *in vivo* generator', *ract*, vol. 100, no. 2, pp. 109–113, Feb. 2012, doi: 10.1524/ract.2011.1841.
[38] K. Bai and A. Wang, 'Polymeric Micelles: Morphology, Synthesis, and Pharmaceutical Application', *E3S Web Conf.*, vol. 290, p. 01029, 2021, doi: 10.1051/e3sconf/202129001029.
[39] U. R. Dahal, A. Prhashanna, and E. E. Dormidontova, 'Hydration of diblock copolymer micelles: Effects of hydrophobicity and co-solvent', *J. Chem. Phys.*, vol. 150, no. 18, p. 184908, May 2019, doi: 10.1063/1.5089251.
[40] H. Otsuka, Y. Nagasaki, and K. Kataoka, 'PEGylated nanoparticles for biological and pharmaceutical applications', *Adv. Drug Deliv. Rev.*, vol. 55, no. 3, pp. 403–419, Feb. 2003, doi: 10.1016/S0169-409X(02)00226-0.

[41] D. J. Sarkar, J. Kumar, N. A. Shakil, T. Adak, and A. C. Watterson, 'Synthesis and Characterization of Amphiphilic PEG Based Aliphatic and Aromatic Polymers and their Self-Assembling Behavior', *J. Macromol. Sci. Part A*, vol. 49, no. 6, pp. 455–465, Jun. 2012, doi: 10.1080/10601325.2012.676845.
[42] M. Ghezzi *et al.*, 'Polymeric micelles in drug delivery: An insight of the techniques for their characterization and assessment in biorelevant conditions', *J. Controlled Release*, vol. 332, pp. 312–336, Apr. 2021, doi: 10.1016/j.jconrel.2021.02.031.
[43] H. Maeda, K. Greish, and J. Fang, 'The EPR Effect and Polymeric Drugs: A Paradigm Shift for Cancer Chemotherapy in the 21st Century', in *Polymer Therapeutics II*, vol. 193, R. Satchi-Fainaro and R. Duncan, Eds. Berlin, Heidelberg: Springer Berlin Heidelberg, 2005, pp. 103–121. doi: 10.1007/12_026.
[44] A. C. Laan, C. Santini, L. Jennings, M. de Jong, M. R. Bernsen, and A. G. Denkova, 'Radiolabeling polymeric micelles for in vivo evaluation: a novel, fast, and facile method', *EJNMMI Res.*, vol. 6, no. 1, p. 12, Dec. 2016, doi: 10.1186/s13550-016-0167-x.
[45] I. Hamley, 'Block Copolymers in Solution: Fundamentals and Applications', p. 302.
[46] A. Leson, V. Filiz, S. Förster, and C. Mayer, 'Water permeation through block-copolymer vesicle membranes', *Chem. Phys. Lett.*, vol. 444, no. 4, pp. 268–272, Aug. 2007, doi: 10.1016/j.cplett.2007.07.023.
[47] W. Verweij, *Calculating CHemical Equilibria in AQuatic Systems*.
[48] S. Brennan, 'Determination of Samarium and Dysprosium Solubility', Wilfrid Laurier University, Canada, 2020.
[49] J. Franciscus Wilhelmus Nijsen, G. Cornelis Krijger, and A. Dirk van het Schip, 'The Bright Future of Radionuclides for Cancer Therapy', *Anticancer Agents Med. Chem.*, vol. 7, no. 3, pp. 271–290, May 2007, doi: 10.2174/187152007780618207.
[50] R. G. Helmer and S. B. Burson, 'Decay of Dy 166 66', *Phys. Rev.*, vol. 119, no. 2, pp. 788–795, Jul. 1960, doi: 10.1103/PhysRev.119.788.
[51] 'Specific activities'. Plexus scientific, nuclear solutions division. [Online]. Available: http://www.iem-inc.com/information/tools/specific-activities

Appendices contents

A. Appendix A: Pathways for the production of ^{166}Ho

There are two main pathways for the production of ^{166}Ho. The first is through the neutron activation (n,γ) of ^{165}Ho, and the second is through the neutron activation (2n,2γ) of ^{164}Dy. Figure 17 illustrates both production methods.

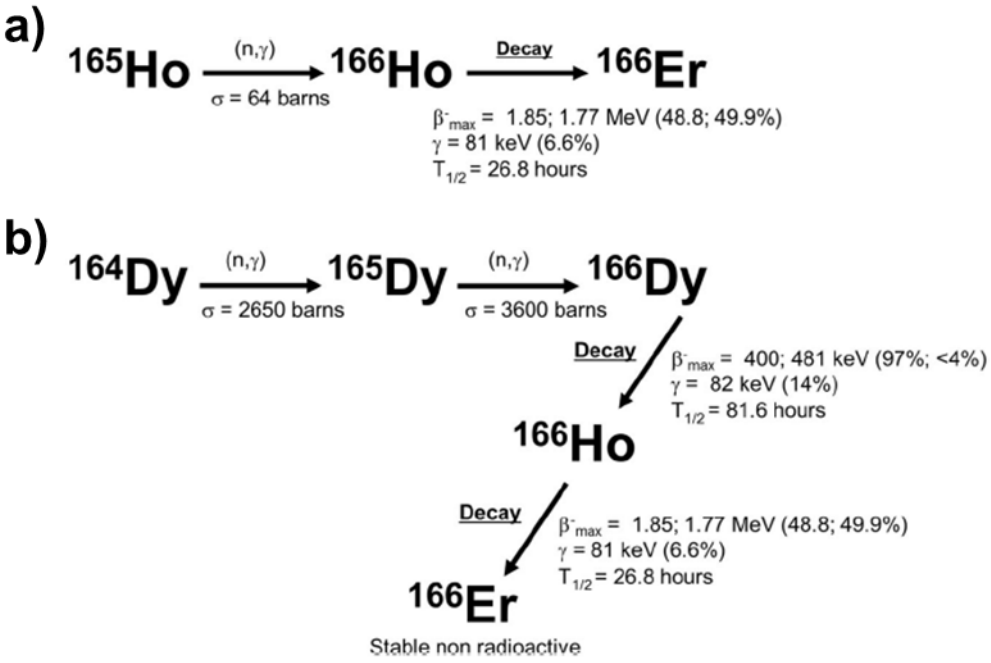

Figure 17. The pathways for the production of 166Ho, via a) the neutron activation of 165Ho and b) the neutron activation of 164Dy. Taken from [3].

Both production methods have their own advantages and disadvantages. The main advantage of producing ^{166}Ho through the irradiation of ^{165}Ho is the high purity of isotope obtained, since ^{165}Ho exists in nature with 100 % abundance [49]. However, from the low cross section, it is possible to say that ^{166}Ho is not as easy to produce from this pathway [49]. Meanwhile, the second pathway is very easy to achieve, due to the very high cross section of both neutron activation reactions for Dy. However, Dy must be enriched to avoid issues with the purity of the Ho, since ^{164}Dy is only 28.2% abundant. Purity issues will also occur due to the β decay of ^{165}Dy, which has a half-life of 2.3 h [50]. This impurity is eliminated through a cooling time after irradiation. When making the *in vivo* generator, Holmium must also be separated from Dysprosium, to keep the system at sub-equilibrium amounts [5]

B. Appendix B: Supplementary information for all CHEAQS speciation calculations.

From [51], the Specific Activity (SA) of ^{166}Ho is $6.90 \times 10^5\ Ci/g$, or $25.5\ GBq/\mu g$. As the activity loss due to the decay process was neglected, adding 50 kBq of this isotope into 1mL of water results in a final concentration of $1.18 \times 10^{-11} M$. Meanwhile, from the Dy concentrations used in the lab, it was possible to calculate a Dy concentration of 0.084 mM for nitrates and 0.074 mM for oxides in HCl. Using this, and defining pH by the presence of hydrogen ions, the results obtained from the CHEAQs software can be found in Table 6-Table 15

Table 6. CHEAQS simulation of metal species and their distribution under optimized pH for different concentrations of Dy(NO3)3

Concentration (M)/species	1,00E-11	1,00E-10	1,00E-09	1,00E-08	1,00E-07	1,00E-06	1,00E-05	2,00E-05	3,00E-05	4,00E-05	5,00E-05	6,00E-05	7,00E-05	8,00E-05	9,00E-05
free Dy 3+	79,24	79,24	79,24	79,24	79,28	79,43	79,91	68,35	45,92	34,69	27,94	23,43	20,20	17,78	15,89
Dy(OH) 2+	20,24	20,24	20,24	20,23	20,20	20,05	19,59	16,52	11,05	8,32	6,67	5,58	4,79	4,20	3,75
Dy(OH)2 +	0,51	0,51	0,51	0,51	0,50	0,50	0,48	0,40	0,27	0,20	0,16	0,13	0,11	0,10	0,09
Dy(OH)3 (aq)	0,02	0,02	0,02	0,02	0,02	0,02	0,02	0,01	0,01	0,01	0,01	0,00	0,00	0,00	0,00
Dy(OH)4 -	0,00	0,00	0,00	0,00	0,00	0,00	0,00	0,00	0,00	0,00	0,00	0,00	0,00	0,00	0,00
Dy(OH)3 (s)	0,00	0,00	0,00	0,00	0,00	0,00	0,00	14,71	42,75	56,78	65,22	70,85	74,88	77,90	80,26

Concentration (M)/species	1,00E-04	2,00E-04	3,00E-04	4,00E-04	5,00E-04	6,00E-04	7,00E-04	8,00E-04	9,00E-04	1,00E-03	1,00E-02	1,00E-01
free Dy 3+	14,38	7,52	5,20	4,02	3,30	2,82	2,47	2,21	2,00	1,84	0,37	0,15
Dy(OH) 2+	3,38	1,72	1,17	0,89	0,72	0,61	0,52	0,46	0,42	0,38	0,05	0,01
Dy(OH)2 +	0,08	0,04	0,03	0,02	0,02	0,01	0,01	0,01	0,01	0,01	0,00	0,00
Dy(OH)3 (aq)	0,00	0,00	0,00	0,00	0,00	0,00	0,00	0,00	0,00	0,00	0,00	0,00
Dy(OH)4 -	0,00	0,00	0,00	0,00	0,00	0,00	0,00	0,00	0,00	0,00	0,00	0,00
Dy(OH)3 (s)	82,15	90,71	93,60	95,06	95,95	96,55	96,98	97,31	97,56	97,77	99,56	99,83

Table 7. CHEAQS simulation of metal species and their distribution under optimized pH for different concentrations of Ho(NO3)3

Concentration (M)/species	1,00E-11	1,00E-10	1,00E-09	1,00E-08	1,00E-07	1,00E-06	2,00E-06	3,00E-06	4,00E-06	5,00E-06	6,00E-06	7,00E-06	8,00E-06	9,00E-06
free Ho 3+	75,19	75,19	75,19	75,19	75,25	75,41	75,52	75,60	64,41	51,62	43,09	36,99	32,42	28,86
Ho(OH) 2+	24,18	24,18	24,18	24,17	24,13	23,97	23,87	23,80	20,23	16,20	13,51	11,59	10,14	9,02
Ho(OH)2 +	0,60	0,60	0,60	0,60	0,60	0,59	0,59	0,59	0,50	0,40	0,33	0,29	0,25	0,22
Ho(OH)3 (aq)	0,02	0,02	0,02	0,02	0,02	0,02	0,02	0,02	0,02	0,01	0,01	0,01	0,01	0,01
Ho(OH)4 -	0,00	0,00	0,00	0,00	0,00	0,00	0,00	0,00	0,00	0,00	0,00	0,00	0,00	0,00
Ho(OH)3 (s)	0,00	0,00	0,00	0,00	0,00	0,00	0,00	0,00	14,85	31,78	43,06	51,13	57,18	61,88

Concentration (M)/species	1,00E-05	2,00E-05	3,00E-05	4,00E-05	5,00E-05	6,00E-05	7,00E-05	8,00E-05	9,00E-05	1,00E-04	1,00E-03	1,00E-02	1,00E-01
free Ho 3+	26,01	13,18	8,88	6,73	5,43	4,56	3,94	3,47	3,10	2,81	0,36	0,07	0,03
Ho(OH) 2+	8,13	4,09	2,74	2,06	1,66	1,39	1,19	1,05	0,93	0,84	0,09	0,01	0,00
Ho(OH)2 +	0,20	0,10	0,07	0,05	0,04	0,03	0,03	0,03	0,02	0,02	0,00	0,00	0,00
Ho(OH)3 (aq)	0,01	0,00	0,00	0,00	0,00	0,00	0,00	0,00	0,00	0,00	0,00	0,00	0,00
Ho(OH)4 -	0,00	0,00	0,00	0,00	0,00	0,00	0,00	0,00	0,00	0,00	0,00	0,00	0,00
Ho(OH)3 (s)	65,65	82,63	88,31	91,16	92,87	94,02	94,84	95,46	95,94	96,33	99,54	99,91	99,96

Table 8. CHEAQS simulation of metal species and their distribution under optimized pH for different concentrations of Dy in a solution containing Cl^- ions

Concentration/ species	1,00E-06	1,00E-05	2,00E-05	3,00E-05	4,00E-05	5,00E-05	6,00E-05	7,00E-05	8,00E-05	9,00E-05	1,00E-04
free Dy 3+	79,87	80,07	69,05	46,03	34,52	27,62	23,02	19,73	17,26	15,34	13,81
Dy(OH) 2+	19,59	19,40	16,60	11,06	8,30	6,64	5,53	4,74	4,15	3,69	3,32
Dy(OH)2 +	0,48	0,47	0,40	0,27	0,20	0,16	0,13	0,11	0,10	0,09	0,08
Dy(OH)3 (aq)	0,02	0,01	0,01	0,01	0,01	0,01	0,00	0,00	0,00	0,00	0,00
Dy(OH)4 -	0,00	0,00	0,00	0,00	0,00	0,00	0,00	0,00	0,00	0,00	0,00
Dy(OH)3 (s)	0,00	0,00	13,91	42,60	56,95	65,56	71,30	75,40	78,48	80,87	82,78

Concentration/ species	2,00E-04	3,00E-04	4,00E-04	5,00E-04	6,00E-04	7,00E-04	8,00E-04	9,00E-04	1,00E-03	1,00E-02	1,00E-01	1,00E+00	1,00E+01
free Dy 3+	6,90	4,60	3,45	2,76	2,30	1,97	1,73	1,53	1,38	0,14	0,01	0,00	0,00
Dy(OH) 2+	1,66	1,11	0,83	0,66	0,55	0,47	0,41	0,37	0,33	0,03	0,00	0,00	0,00
Dy(OH)2 +	0,04	0,03	0,02	0,02	0,01	0,01	0,01	0,01	0,01	0,00	0,00	0,00	0,00
Dy(OH)3 (aq)	0,00	0,00	0,00	0,00	0,00	0,00	0,00	0,00	0,00	0,00	0,00	0,00	0,00
Dy(OH)4 -	0,00	0,00	0,00	0,00	0,00	0,00	0,00	0,00	0,00	0,00	0,00	0,00	0,00
Dy(OH)3 (s)	91,39	94,26	95,70	96,56	97,13	97,54	97,85	98,09	98,28	99,83	99,98	100,00	100,00

Table 9. CHEAQS simulation of metal species and their distribution under optimized pH for different concentrations of Ho in a solution containing Cl^- ions

Concentration/ species	1,00E-07	1,00E-06	2,00E-06	3,00E-06	4,00E-06	5,00E-06	6,00E-06	7,00E-06	8,00E-06	9,00E-06	1,00E-05
free Ho 3+	75,89	75,92	75,95	75,98	66,85	53,48	44,56	38,20	33,42	29,71	26,74
Ho(OH) 2+	23,47	23,44	23,42	23,39	20,57	16,45	13,71	11,75	10,28	9,14	8,23
Ho(OH)2 +	0,57	0,57	0,57	0,57	0,50	0,40	0,33	0,29	0,25	0,22	0,20
Ho(OH)3 (aq)	0,02	0,02	0,02	0,02	0,02	0,01	0,01	0,01	0,01	0,01	0,01
Ho(OH)4 -	0,00	0,00	0,00	0,00	0,00	0,00	0,00	0,00	0,00	0,00	0,00
Ho(OH)3 (s)	0,00	0,00	0,00	0,00	12,03	29,63	41,35	49,73	56,02	60,90	64,81

Concentration/ species	2,00E-05	3,00E-05	4,00E-05	5,00E-05	6,00E-05	7,00E-05	8,00E-05	9,00E-05	1,00E-04	1,00E-03	1,00E-02	1,00E-01
free Ho 3+	13,37	8,91	6,68	5,35	4,46	3,82	3,34	2,97	2,67	0,27	0,03	0,00
Ho(OH) 2+	4,11	2,74	2,06	1,65	1,37	1,18	1,03	0,91	0,82	0,08	0,01	0,00
Ho(OH)2 +	0,10	0,07	0,05	0,04	0,03	0,03	0,02	0,02	0,02	0,00	0,00	0,00
Ho(OH)3 (aq)	0,00	0,00	0,00	0,00	0,00	0,00	0,00	0,00	0,00	0,00	0,00	0,00
Ho(OH)4 -	0,00	0,00	0,00	0,00	0,00	0,00	0,00	0,00	0,00	0,00	0,00	0,00
Ho(OH)3 (s)	82,41	88,27	91,20	92,96	94,14	94,97	95,60	96,09	96,48	99,65	99,96	100,00

Table 10. CHEAQS simulation results of metal species and their distribution with a constant Dy concentration of 0.084 mM, and a constant NO_3^- concentration of 0.252 mM for varying pH values

pH/Species	0	1	2	3	4	5	6	7	8	9	10	11	12	13	14
free Dy 3+	99,99	99,99	99,98	99,97	99,94	99,94	98,80	98,32	97,64	88,10	18,36	0,00	0,00	0,00	0,00
Dy(OH) 2+	0,00	0,00	0,00	0,00	0,02	0,02	1,16	1,64	2,32	11,71	55,79	0,00	0,00	0,00	0,00
Dy(OH)2 +	0,00	0,00	0,00	0,00	0,00	0,00	0,00	0,00	0,01	0,16	17,22	0,00	0,00	0,00	0,00
Dy(OH)3 (aq)	0,00	0,00	0,00	0,00	0,00	0,00	0,00	0,00	0,00	0,00	7,04	0,94	0,07	0,01	0,00
Dy(OH)4 -	0,00	0,00	0,00	0,00	0,00	0,00	0,00	0,00	0,00	0,00	1,50	99,06	99,93	100,00	99,99
Dy(NO3) 2+	0,01	0,02	0,03	0,04	0,04	0,04	0,04	0,04	0,04	0,04	0,01	0,00	0,00	0,00	0,00

Table 11. CHEAQS simulation results of metal species and their distribution with 500 kBq of ^{166}Ho for varying pH values

pH/Species	0	1	2	3	4	5	6	7	8	9	10	11	12	13	14
free Ho 3+	100,00	100,00	99,99	99,98	99,95	99,67	96,96	75,99	19,83	0,14	0,00	0,00	0,00	0,00	0,00
Ho(OH) 2+	0,00	0,00	0,00	0,00	0,03	0,31	3,02	23,42	60,42	4,40	0,01	0,00	0,00	0,00	0,00
Ho(OH)2 +	0,00	0,00	0,00	0,00	0,00	0,00	0,01	0,57	14,52	10,56	0,19	0,00	0,00	0,00	0,00
Ho(OH)3 (aq)	0,00	0,00	0,00	0,00	0,00	0,00	0,00	0,02	4,52	32,84	5,92	0,63	0,06	0,01	0,00
Ho(OH)4 -	0,00	0,00	0,00	0,00	0,00	0,00	0,00	0,00	0,72	52,04	93,87	99,36	99,93	100,00	99,99
Ho(NO3) 2+	0,00	0,01	0,02	0,02	0,02	0,02	0,02	0,02	0,00	0,00	0,00	0,00	0,00	0,00	0,00

Table 12. CHEAQS results of metal species and their distribution with a constant Dy concentration of 0.074 mM, and a constant Cl^- concentration of 0.1 mM for varying pH values

pH/species	0	1	2	3	4	5	6	7	8	9	10	11	12	13	14
free Dy 3+	99,99	99,99	99,97	99,95	99,93	99,72	98,73	98,20	97,41	86,55	14,30	0,00	0,00	0,00	0,00
Dy(OH) 2+	0,00	0,00	0,00	0,00	0,02	0,23	1,22	1,75	2,53	13,20	53,26	0,00	0,00	0,00	0,00
Dy(OH)2 +	0,00	0,00	0,00	0,00	0,00	0,00	0,00	0,00	0,01	0,21	19,99	0,00	0,00	0,00	0,00
Dy(OH)3 (aq)	0,00	0,00	0,00	0,00	0,00	0,00	0,00	0,00	0,00	0,00	9,86	0,89	0,07	0,01	0,00
Dy(OH)4 -	0,00	0,00	0,00	0,00	0,00	0,00	0,00	0,00	0,00	0,00	2,52	99,12	99,93	100,00	99,99
DyCl 2+	0,01	0,02	0,04	0,05	0,05	0,06	0,05	0,05	0,05	0,05	0,01	0,00	0,00	0,00	0,00
DyCl2 +	0,00	0,00	0,00	0,00	0,00	0,00	0,00	0,00	0,00	0,00	0,00	0,00	0,00	0,00	0,00

Table 13. CHEAQS simulation results of metal species and their distribution with 500 kBq of ^{166}Ho for varying pH values

pH/species	0	1	2	3	4	5	6	7	8	9	10	11	12	13	14
free Ho 3+	99,99	99,99	99,97	99,94	99,92	99,63	96,92	75,96	19,83	0,14	0,00	0,00	0,00	0,00	0,00
Ho(OH) 2+	0,00	0,00	0,00	0,00	0,03	0,31	3,02	23,41	60,42	4,40	0,00	0,00	0,00	0,00	0,00
Ho(OH)2 +	0,00	0,00	0,00	0,00	0,00	0,00	0,01	0,57	14,52	10,56	0,00	0,00	0,00	0,00	0,00
Ho(OH)3 (aq)	0,00	0,00	0,00	0,00	0,00	0,00	0,00	0,02	4,52	32,84	0,00	0,63	0,06	0,01	0,00
Ho(OH)4 -	0,00	0,00	0,00	0,00	0,00	0,00	0,00	0,00	0,72	52,04	0,00	99,36	99,93	100,00	99,99
HoCl 2+	0,01	0,02	0,04	0,05	0,06	0,06	0,06	0,05	0,01	0,00	0,00	0,00	0,00	0,00	0,00
HoCl2 +	0,00	0,00	0,00	0,00	0,00	0,00	0,00	0,00	0,00	0,00	0,00	0,00	0,00	0,00	0,00

Table 14. CHEAQS simulation of metal species and their distribution under optimized pH and a constant concentration of Dy(NO3)3 of 0.085 mM for different concentrations of phosphate ions

Phosphate concentration/Species	1,00E-11	1,00E-10	1,00E-09	1,00E-08	1,00E-07	1,00E-06	1,00E-05	2,00E-05	3,00E-05
free Dy 3+	98,32	98,32	98,32	98,31	98,20	97,14	86,51	74,72	62,93
Dy(OH) 2+	1,64	1,64	1,64	1,64	1,64	1,63	1,54	1,43	1,32
Dy(OH)2 +	0,00	0,00	0,00	0,00	0,00	0,00	0,00	0,00	0,00
Dy(OH)3 (aq)	0,00	0,00	0,00	0,00	0,00	0,00	0,00	0,00	0,00
Dy(OH)4 -	0,00	0,00	0,00	0,00	0,00	0,00	0,00	0,00	0,00
Dy(PO4) (s)	0,00	0,00	0,00	0,01	0,12	1,19	11,90	23,81	35,71

Phosphate concentration/Species	4,00E-05	5,00E-05	6,00E-05	7,00E-05	8,00E-05	9,00E-05	1,00E-04	1,00E-03	1,00E-02
free Dy 3+	51,16	39,40	27,67	15,98	4,41	0,00	0,00	0,00	0,00
Dy(OH) 2+	1,19	1,05	0,88	0,66	0,34	0,00	0,00	0,00	0,00
Dy(OH)2 +	0,00	0,00	0,00	0,00	0,00	0,00	0,00	0,00	0,00
Dy(OH)3 (aq)	0,00	0,00	0,00	0,00	0,00	0,00	0,00	0,00	0,00
Dy(OH)4 -	0,00	0,00	0,00	0,00	0,00	0,00	0,00	0,00	0,00
Dy(PO4) (s)	47,62	59,52	71,43	83,34	95,24	100,01	100,01	100,00	100,00

Table 15. CHEAQS simulation of metal species and their distribution under optimized pH and a constant concentration of Dy of 0.085 mM and a constant Cl^- concentration of 0.1 mM, for different concentrations of phosphate ions

Phosphate concentration/Species	1,00E-11	1,00E-10	1,00E-09	1,00E-08	1,00E-07	1,00E-06	1,00E-05	2,00E-05	3,00E-05
free Dy 3+	97,45	97,46	97,45	97,42	97,19	94,78	70,80	44,23	17,84
Dy(OH) 2+	2,49	2,49	2,49	2,49	2,49	2,46	2,12	1,68	1,05
Dy(OH)2 +	0,01	0,01	0,01	0,01	0,01	0,01	0,01	0,01	0,01
Dy(OH)3 (aq)	0,00	0,00	0,00	0,00	0,00	0,00	0,00	0,00	0,00
Dy(OH)4 -	0,00	0,00	0,00	0,00	0,00	0,00	0,00	0,00	0,00
Dy(PO4) (s)	0,00	0,00	0,00	0,03	0,27	2,70	27,03	54,05	81,08

Phosphate concentration/Species	4,00E-05	5,00E-05	6,00E-05	7,00E-05	8,00E-05	9,00E-05	1,00E-04	1,00E-03	1,00E-02
free Dy 3+	0,00	0,00	0,00	0,00	0,00	0,00	0,00	0,00	0,00
Dy(OH) 2+	0,00	0,00	0,00	0,00	0,00	0,00	0,00	0,00	0,00
Dy(OH)2 +	0,00	0,00	0,00	0,00	0,00	0,00	0,00	0,00	0,00
Dy(OH)3 (aq)	0,00	0,00	0,00	0,00	0,00	0,00	0,00	0,00	0,00
Dy(OH)4 -	0,00	0,00	0,00	0,00	0,00	0,00	0,00	0,00	0,01
Dy(PO4) (s)	100,01	100,01	100,01	100,01	100,01	100,01	100,01	100,01	100,00

C. Appendix C: kinetic study: the effect of labelling time on loading

While performing the kinetics study that resulted in **Figure 5**, another parameter of interest was the time allowed for stirring after the addition of the active ^{166}Dy/Ho. If the loading mechanism is diffusion based, it is expected that it will reach a plateau at a certain point in time, where changes in loading efficiency cease to be significant. Taking this into account, the objective of this study was to ensure that the plateau was already reached with a 30 min process under stirring, and the loading efficiency would not increase significantly if the process time was increased to one hour. The results are shown in Figure 18.

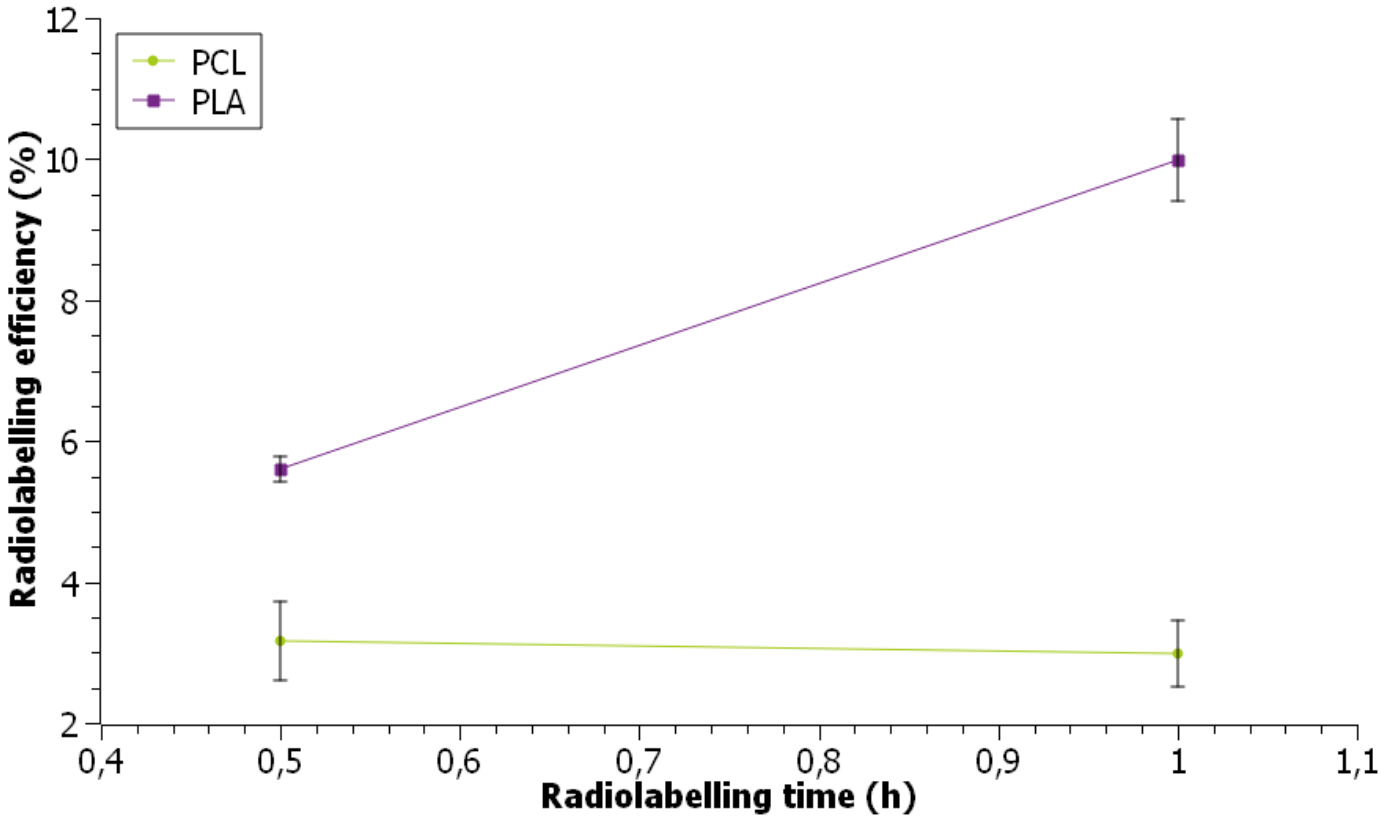

Figure 18. Radiolabelling efficiency achieved as a function of time allowed for radiolabelling in PCL-PEO micelles (in green) and PLA-PEO micelles (in purple). (Activity per ml of micelle solution: 1 kBq/ml, Dy concentration: 0.084 mM, polymer concentration: 4.3 mg/ml for PEO-PCL micelles and 2.5 mg/ml for PEO-PLA micelles in 10 mM HEPES buffer with pH of 7.4, radiolabelling time: 30 minutes and an hour under stirring)

As seen on Figure 18, there is no significant increase in the radiolabelling efficiency achieved after one hour of stirring compared to 30 minutes stirring. Because of this, and due to the results obtained in the concentration study

(shown in **Figure 5**) a decision was made to proceed with other types of experiments, such as exploring the addition of phosphates into the system.

Because both radiolabelling efficiencies and stabilities were quite low, the next step was decided to perform a study on the effect of different activities (and therefore metal concentrations) on the radiolabelling efficiency in both PCL-PEO and PLA-PEO micelles. The results can be seen in Figure 19.

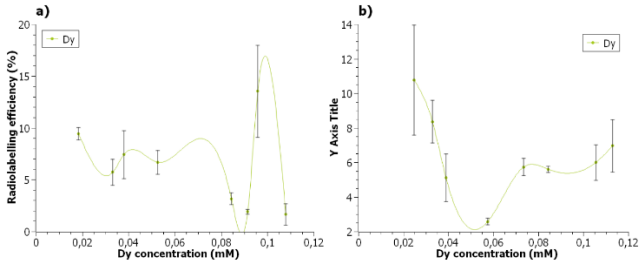

Figure 19. Radiolabelling efficiency as a function of Dy concentration for a) PCL-PEO micelles, and b) PLA-PEO micelles. (Polymer concentration: 4.3 mg/ml for PEO-PCL micelles and 2.5 mg/ml for PEO-PLA micelles in 10 mM HEPES buffer with pH of 7.4, radiolabelling time: 30 minutes under stirring)

Figure 19 does not really show a clear pattern when it comes to radiolabelling efficiency as a function of concentration. This may be explained by the low metal concentrations added when adding such low activities (the maximum concentration used in these experiments is 0.12 mM) where, although precipitation is already expected, according to Figure 6, but it is not yet the dominant species, so it is possible that metal ions present inside the micelle core have not reached the needed concentration to precipitate. This would lead free metal ions to come out of the micelles. This is supported by the large standard deviation between replicates seen in many results, especially in Figure 19 a).

D. Appendix D: Dependence of active metal stock pH on loading

On the first attempt at radiolabelling micelles with active Dy_zO_3 dissolved in pH 1 HCl, a surprising development occurred, as loading efficiencies were extremely low, as seen in Figure 20.

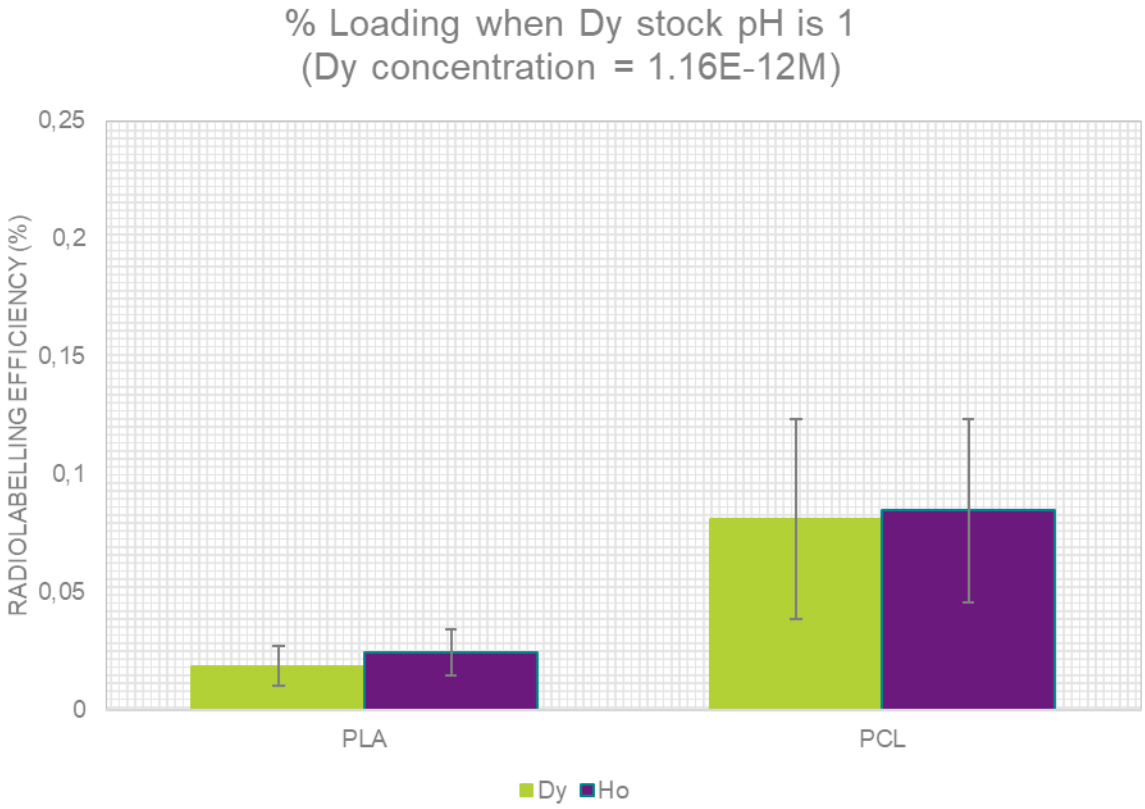

Figure 20. The radiolabelling efficiency achieved on the first use of a Dy_2O_3 in HCl source, where stock pH was 1. (Activity per ml of micelle solution: 10 kBq/ml or 7.08 pM, polymer concentration: 4.3 mg/ml for PEO-PCL micelles and 2.5 mg/ml for PEO-PLA micelles in 10 mM HEPES buffer with pH of 7.4, radiolabelling time: 30 minutes under stirring)

From Figure 20, it is possible to see that radiolabelling efficiencies in this set of experiments were lower than 0.2%. From the investigation performed by Liu et al., where different system pH were used to further experiment with the loading mechanism, it was found that acidic systems, where free metallic ions were the dominant metal species, and in the case of Lu, all of the metal speciated to the free ions, low radiolabelling efficiencies would result. Therefore, it was concluded that this was probably indicating that the amount of stock active metal solution added was enough to shift the micelle solution pH regardless of the HEPES buffer that was added to keep the pH at 7.4. This led to the decision to slightly neutralize the stock solution, to a pH that would not induce precipitation (as the stock solution will precipitate if the pH is higher than 6). However, as the most desirable stock pH was unknown, an experiment was made to optimize the stock pH for all future experiments. The results can be seen in Figure 21.

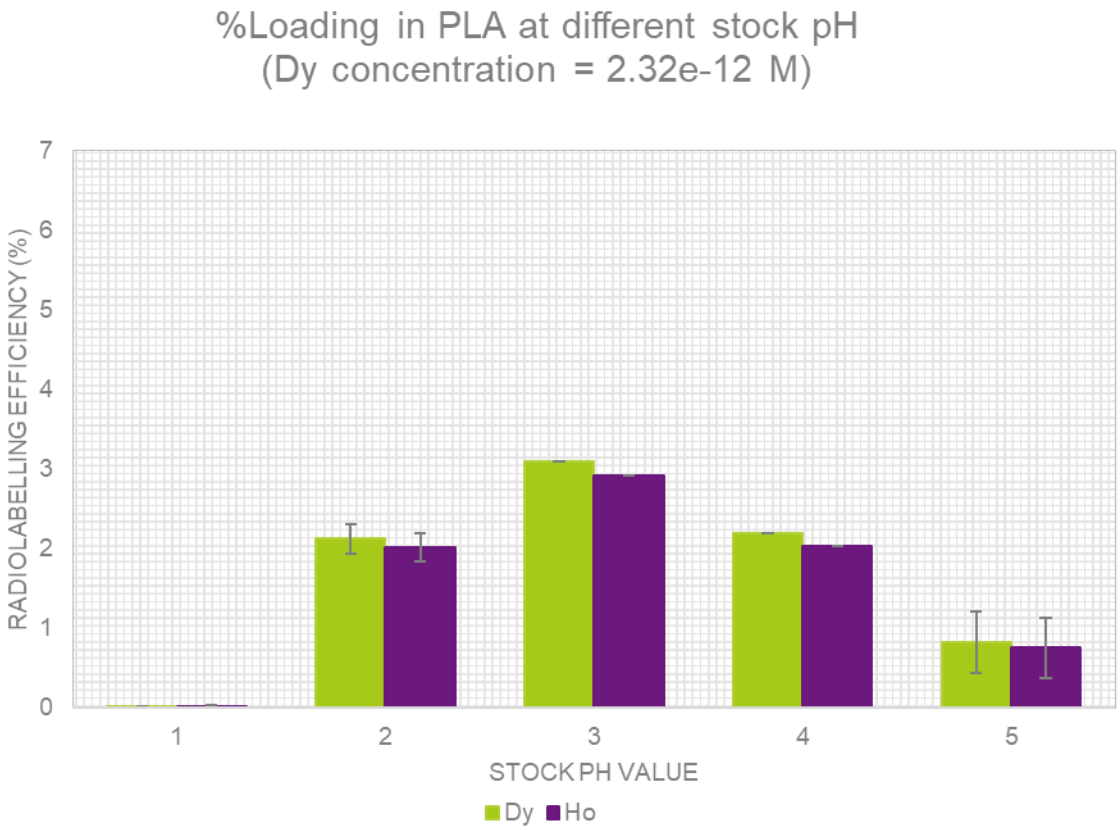

Figure 21. The radiolabelling efficiency achieved in PLA-PEO micelles as a function of stock pH. (Activity per ml of micelle solution: 10 kBq/ml or 7.08 pM, polymer concentration: 2.5 mg/ml for PEO-PLA micelles in 10 mM HEPES buffer with pH of 7.4, radiolabelling time: 30 minutes under stirring)

From Figure 21, it is possible to see that the optimal stock pH for the experiments made was 3, as it showed the highest radiolabelling efficiency. Thus, it was decided that for all future experiments that required the use of the Dy_2O_3 in HCl activity source, the source would be neutralized prior to attempting radiolabelling, as explained in section 3.2.2.3.